Available online at www.sciencedirect.com
ScienceDirect
Journal of Power Sources 173 (2007) 375–393
JOURNAL OF POWER SOURCES
www.elsevier.com/locate/jpowsour

A two-dimensional steady state model including the effect of liquid water for a PEM fuel cell cathode

R. Madhusudana Rao [a], D. Bhattacharyya [a], R. Rengaswamy [a,*], S.R. Choudhury [b]

[a] *Department of Chemical Engineering, Clarkson University, Potsdam, NY 13699, USA*
[b] *Naval Materials Research Laboratory, Ambernath, Maharashtra, India*

Received 4 January 2007; received in revised form 19 April 2007; accepted 19 April 2007
Available online 27 April 2007

Abstract

A two-dimensional steady state model for a PEM fuel cell cathode is described in this work. All the components in the cathode such as the gas manifold, diffusion layer, microporous layer and the catalyst layer are modeled. The effect of the liquid water is taken into account in every layer of the cathode. The model was developed and simulated using a combination of Maple and MATLAB. The combination provides a flexible framework for quickly developing models with various assumptions and different complexities. The cathode catalyst layer was modeled using both macrohomogeneous and spherical agglomerate characterizations. The model is validated using experimental data. During model validation, various assumptions are considered for transport within the porous layers of the cathode. Subsequently, the assumptions and characteristics that best predicts the experimental data are highlighted. The major conclusion of this work is that a model that includes liquid water in all the layers with a flooded spherical agglomerate characterization for the reaction layer best predicts the PEM fuel cell behavior in terms of an *i*–*v* characterization for a wide range of reactant flow rates. The utility of the steady state model for the optimization of the cathode catalyst layer design parameters is also described.

Keywords: PEMFC; PEM fuel cell; Steady state model; Spherical agglomerate characterization; Macrohomogeneous characterization

1. Introduction

There is considerable interest in the modeling of proton exchange membrane fuel cells (PEMFC), and a number of PEMFC models have been proposed in the literature over the last two decades. Models proposed during the early years were typically one-dimensional and accounted for steady state mass transport and electrochemical kinetics. Subsequently, both simplified and complex models in terms of dimensionality and physicochemical phenomena have been studied. These models have been used for a variety of purposes such as, prediction of the typical characteristic (current–potential) curves, parameter and operating conditions sensitivity analysis, and three-dimensional temperature, pressure and species concentration distributions in the case of fuel cell stacks.

There are two main approaches that have been pursued in the modeling of PEMFCs. One is the detailed models of transport processes and electrochemical reactions that take place in a fuel cell. The other approach is the development of simplified models with well defined reactor conditions for correlation of fuel cell operation as exemplified by the work of [1]. In this paper, we follow the former approach. Our aim here is the development of a model that can be used for detailed analysis and optimization of fuel cell systems. This would entail including the effect of liquid water in all the layers of the fuel cell. Further, we also require that the experimental parameters to be correlated to the fuel cell performance. Development of such a detailed modeling and computational approach would allow for comprehensive phenomenological study of several important factors as outlined excellently in [2].

A review of state-of-the-art in models proposed for PEM fuel cells is presented in the next section. A detailed review of the present status of fundamental models for fuel cell engineering is also presented in [3]. The review highlighted the current status of hydrogen/air polymer electrolyte fuel cells (PEFCs),

* Corresponding author. Tel.: +1 315 268 4423; fax: +1 315 268 6654.
E-mail addresses: raghu@clarkson.edu, rengasam@che.iitb.ernet.in (R. Rengaswamy).

0378-7753/$ – see front matter © 2007 Published by Elsevier B.V.
doi:10.1016/j.jpowsour.2007.04.053

Nomenclature

a_a	effective area of the catalyst per unit volume of the catalyst layer (m^2 Pt m^{-3})
a_{pt}	specific area of Pt (m^2 Pt kg^{-1} Pt^{-1})
a_{RL}	area of cross section of the catalyst layer (m^2)
a_w	activity of water inside the ionomer phase
a_1	surface area of agglomerates per unit volume of catalyst layer (m^{-1})
$C_{i,k}$	concentration of species i in region k (gmol m^{-3})
C_{io}	inlet concentrations of O_2, N_2 and H_2O (gmol m^{-3})
$C_{O_2,mem}$	concentration of dissolved oxygen inside the ionomer (mol m^{-3})
$C_{O_2\|ns}$	concentration of dissolved oxygen at the ionomer and the spherical agglomerate interface (mol m^{-3})
$C^s_{O_2}$	saturation concentration of oxygen inside the ionomer pores (mol m^{-3})
$D_{i,effd}$	effective diffusivity of species i in the diffusion layer (m^2 s^{-1})
$D_{i,effm}$	effective diffusivity of species i in the microporous layer (m^2 s^{-1})
$D_{i,effr}$	effective diffusivity of species i in the catalyst layer (m^2 s^{-1})
$D_{O_2,mem}$	diffusivity of dissolved oxygen in the ionomer pores (m^2 s^{-1})
$D_{O_2,w}$	diffusivity of oxygen in liquid water (m^2 s^{-1})
$D^{eff}_{O_2,mem}$	effective diffusivity of dissolved oxygen in ionomer pores (m^2 s^{-1})
f_{mem}	weight fraction of ionomer inside the catalyst layer
f_{pt}	weight fraction of platinum on carbon
F	Faraday's constant (C g^{-1} equiv.$^{-1}$)
F_{air}	cathode inlet flow rate (lpm)
h_{ch}	height of the gas channels (m)
$H_{O_2,mem}$	Henry's constant for air–ionomer interface (atm m^3 mol^{-1})
$H_{O_2,w}$	Henry's constant for air–water interface (atm m^3 mol^{-1})
i_a	local current density (A m^{-2} Pt^{-1})
i_{cell}	cell current density (A m^{-2})
i_o	exchange current density for oxygen reduction on Pt (A m^{-2} Pt^{-1})
$\mathbf{j}_r$	local current density inside the catalyst layer (A m^{-2})
$\mathbf{J}_i$	local flux due to diffusion of species i (mol m^{-2} s)
k_c	condensation rate constant (s^{-1})
k_{rxn}	rate constant for oxygen reduction reaction (s^{-1})
k_v	evaporation rate constant (atm^{-1} s^{-1})
K_w	permeability of liquid water inside porous regions (m^2)
K_{wo}	permeability of liquid water inside porous regions at 100% saturation (m^2)
K_1, K_2, K_3	constants for interface saturation
L	length of the gas flow channels (m)
m_{pt}	platinum loading inside the catalyst layer (kg Pt m^{-2} RL^{-1})
M_w	molecular weight of water (g mol^{-1})
n_{ch}	number of gas flow channels in a single graphite plate
n_e	number of electrons taking part in the oxygen reduction reaction
$\mathbf{N}_{w,k}$	flux of liquid water in region k (mol m^{-2} s)
$p_{i,k}$	partial pressure of species i in region k (atm)
p_w	partial pressure of water vapor (atm)
p^{sat}_w	saturation pressure of water vapor (atm)
P_c	capillary pressure (atm)
P_{cat}	cathode inlet pressure (atm)
P_g	total pressure of the gas phase (atm)
P_l	pressure of liquid water (atm)
q	switching function
r_{agg}	radius of the agglomerate (m)
R	universal gas constant (J mol^{-1} K^{-1})
R_{O_2}	rate of oxygen reduction reaction per unit volume of the catalyst layer (mol m^{-3} s^{-1})
R_w	interfacial transfer of water between liquid and vapor (mol m^{-2} s^{-1})
RH_{air}	relative humidity of cathode inlet air (%)
s_k	liquid water saturation level in region k
t_{GDL}	thickness of the gas diffusion layer (m)
t_{MPL}	thickness of the microporous layer (m)
t_{RL}	thickness of the catalyst layer (m)
T_{air}	cathode inlet air temperature (K)
T_{cell}	cathode temperature (K)
u_{inlet}	velocity at the inlet to gas flow channels (m s^{-1})
$\mathbf{u}_l$	liquid water velocity vector (m s^{-1})
v_c	volume occupied by the carbon inside catalyst layer (m^3)
v_{mem}	volume occupied by the ionomer inside catalyst layer (m^3)
v_{pt}	volume occupied by the platinum inside catalyst layer (m^3)
v_{RL}	volume of the catalyst layer (m^3)
v_s	volume of solids inside the catalyst layer (m^3)
v_v	void volume inside the catalyst layer (m^3)
V_{cat}	cathode potential measured against SHE (V)
V_{oc}	open circuit potential measured against SHE (V)
w_c	mass of carbon inside the agglomerate (kg)
w_{cell}	width of the cathode (m)
w_{ch}	width of the gas flow channels (m)
w_{mem}	mass of ionomer inside the agglomerate (kg)
w_{pt}	mass of platinum inside the catalyst layer (kg)
y_w	mole fraction of water vapor in the gas phase

Greek letters

α	transfer coefficient
δ_{mem}	thickness of ionomer film covering the agglomerate (m)

δ_w	thickness of water layer on top of the agglomerate (m)
ϵ_d	void fraction inside the gas diffusion layer
ϵ_m	void fraction inside the microporous layer
ϵ_k	void fraction inside region k
ϵ_{mem}	fraction of volume occupied by the ionomer inside the catalyst layer
ϵ_r	void fraction inside the catalyst layer
ζ	effectiveness factor
η_r	local overpotential inside the catalyst layer (V)
θ	contact angle
κ_{eff}	effective conductivity of ionomer inside the catalyst layer (mho m^{-1})
κ_{mem}	conductivity of ionomer (mho m^{-1})
λ_{O_2}	oxygen excess ratio
λ_w	water content inside the ionomer (mol H_2O (mol SO_3^-)$^{-1}$)
μ_w	viscosity of liquid water (kg m^{-1} s^{-1})
ρ_c	density of carbon (kg m^{-3})
ρ_{mem}	density of ionomer (kg m^{-3})
ρ_{pt}	density of platinum (kg m^{-3})
ρ_w	density of liquid water (kg m^{-3})
ϕ_r	local ionomer potential inside the catalyst layer (V)
ψ	Thiele modulus

Subscripts

i	index for the species: O_2, N_2, H_2O
k	index for the region: gas flow channel, diffusion layer, microporous layer and catalyst layer

direct methanol fuel cells (DMFCs), and solid oxide fuel cells (SOFCs). Our main observation on the detailed models available in the literature is that most of these models do not characterize the effect of liquid water on the fuel cell performance. Comprehensive models that include the effect of liquid water in our view are the ones proposed by [4–6]. Pasaogullari and Wang [4] describe the governing physics of water transport in both hydrophilic and hydrophobic diffusion media along with one-dimensional analytical solutions of related transport processes. They report that the liquid water transport across the gas diffusion layer (GDL) is controlled by capillary forces resulting from the gradient in phase saturation. A one-dimensional analytical solution of liquid water transport across the GDL was derived. Effect of GDL wettability on liquid water transport was explored in detail for the first time. Furthermore, the authors also investigate the effect of flooding on oxygen transport and cell performance and show that flooding diminishes the cell performance as a result of decreased oxygen transport and surface coverage of active catalyst by liquid water. Lin et al. [5] model the liquid water in the gas diffusion and catalyst layers and they characterize the catalyst layer through a cylindrical geometry. Their model domain consists of the membrane, the cathode catalyst layer and the cathode diffusion layer. Further, experimental studies have shown that the catalyst layer in PEMFC is better characterized by spherical agglomerates, see Fig. 1[7]. In the work of [6], liquid water is modeled in all the layers including the manifold. However, the catalyst layer is not characterized and a macrohomogeneous approach is used. We later show with experimental data that this would lead to a poor prediction of fuel cell behavior in certain operational regimes.

In this work, the first major contribution is a model that includes liquid water in all the layers of the cathode (gas manifold, gas diffusion layer, microporous layer and the catalyst layer) and the catalyst layer is characterized as spherical agglomerates, in line with the experimental evidence [7–9]. Further, we compare several models with different simplifications and show the importance of modeling the liquid water in all the layers with the correct characterization of the catalyst layer. Cathode experimental data for a wide range of flow rates is used to validate and evaluate the proposed models. Our main conclusion is that when the catalyst layer is characterized using spherical agglomerates with liquid water effects, and the transport in the porous regions is by diffusion in the bulk, the model predictions match very well with experimental data for the entire polarization range and at various flow rates.

The second major contribution of this work is the correlation of the experimental variables used in the preparation of the membrane electrode assembly (MEA) to the model parameters. This correlation is derived based on a spherical agglomerate characterization of the reaction layer. Hence, once the experimental variables used in the preparation of the MEA such as

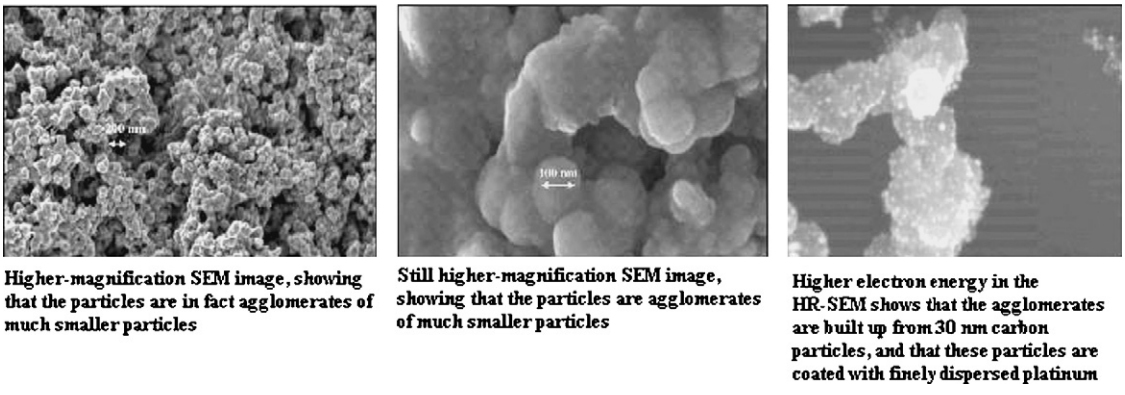

Fig. 1. Scanning electron microscope (SEM) images of PEM fuel cell electrode [7].

the thickness of the catalyst layer (t_{RL}), the catalyst loading (m_{pt}), the weight fraction of platinum on carbon (f_{pt}), the weight fraction of ionomer inside the catalyst layer (f_{mem}), and the density of ionomer (ρ_{mem}) are provided, all the other model parameters are derived through balance equations. For example, the void fractions and the thickness of the ionomer layer covering the agglomerates are related to the experimental parameters. This directly ties in the model predictions to the experimental characterization. We believe that this is of major importance because directly usable multi-parameter optimization studies are possible with this model. The results of such an optimization study have been reported in another paper [10].

2. Literature review

Recent literature is abundant with a variety of PEMFC models. Both simplified and complex models in terms of dimensionality and physicochemical phenomena have been studied [11–43]. Seminal papers in PEMFC modeling were published by Springer et al. [36] and Bernardi and Verbrugge [11,12] and in contemporary literature, significant contributions were made by [4,44]. A common feature in most of these models is that the reaction or catalyst layer is not modeled in detail. The reaction layer is treated as an ultra-thin layer, thus neglecting the transport of reactant gases and products. Hence, the catalyst layer is treated as a source/sink boundary condition for transport equations in the gas diffusion layer. Contrary to this assumption, even if gas phase transport is neglected on the consideration of an ultra-thin layer, the presence of ionomer in the reaction layer along with carbon and platinum makes transport within the pores of the ionomer important. Moreover, catalyst layer is the region where various limiting mechanisms can occur and thus, can have a strong influence on the overall performance of the cell.

As gas diffusion electrodes (GDEs) are difficult to characterize, one of the first assumptions that was made to model them was the concept of "flooded agglomerates", introduced by Giner and Hunter [45]. They have considered cylindrical geometry for the agglomerates. Results were presented for alkaline oxygen electrode. The potential drop was assumed to change only in the axial direction and diffusion of the dissolved gases was assumed to be in the radial direction of the agglomerates. The effect of the cylindrical agglomerate radius on the current generated and its distribution were studied. Porous GDEs with the same assumptions have been extended to model the phosphoric acid fuel cells (PAFC) cathode and anode in detail [47,46]. Various transport and kinetic processes which take place in the porous electrodes were taken into account. The model was used in the simulation mode for predictive analysis and for electrode development process.

One of the drawbacks with the above-proposed flooded-agglomerate model is that it does not consider any tortuosity for the gas phase transport as the agglomerates are assumed to completely extend from the gas side to the electrolyte side. The cylindrical flooded-agglomerate model was modified by Celiker et al. [48] considering spherical geometry. They have investigated their model predictions by considering the cathodic reduction of oxygen in alkaline medium. Subsequently, many studies conducted by various researchers with the spherical flooded-agglomerate model were presented for alkaline fuel cells (AFC) [49,50] and PAFC [50–52].

Even in the case of PEM fuel cells, researchers have studied the effect of various phenomena in the catalyst layer based on flooded-agglomerate model [50,53–57]. Perry et. al. [50] have developed a model for gas diffusion electrode that can be used as a diagnostic tool for designing of fuel cells. This is a one-dimensional model for mass transport in the zone where Tafel kinetics is valid. The models presented were generally valid for any GDE with either liquid electrolyte (AFC and PAFC) or ion-exchange membrane (PEMFC). The model was used to study the effects of mass-transport limitations on the polarization characteristics of oxygen reduction reaction in the cathode. Using negligible mass transfer resistance in the gas phase the model develops a function for evaluating the Thiele modulus for the catalyst-binder agglomerates. These relations along with ion transport equations are combined to develop a single variable second order differential equation. For this equation, asymptotic solutions were developed at different limiting conditions. The model also predicts different Tafel slopes for distinct regions. The authors have also shown how the results may be used as a diagnostic tool for analyzing fuel cell cathode data. Siegel et al. [54] have proposed a steady state two-dimensional PEMFC model based on agglomerate geometry for the catalyst layer. The agglomerates are characterized by mean diameter and a characteristic length. Based on the model results, it has been highlighted that the fuel cell performance is highly dependent on catalyst structure. Wang et al. [56] have investigated transport and reaction kinetics in spherical agglomerates of cathode catalyst layer. They have considered two types of spherical agglomerates: the first one consisting of a mixture of carbon/catalyst particles and perfluorosulfonated ionomer (PFSI) and the other type consisting of carbon/catalyst particles and water-filled pores. The model has been used to study current conversion, reactant and current distribution and catalyst utilization. However, most of these models do not treat liquid water in the catalyst layer. Further these models ignore the other layers in an electrode.

One of the probable reasons for neglecting reaction layer in PEMFC models published in the beginning could be lack of instrumentation to characterize its morphology accurately. With the availability of advanced microscopy instruments like scanning electron microscope (SEM) and transmission electron microscope (TEM), researchers have been able to study the morphology of complex nanostructures such as, PEM fuel cell electrodes. Middleman [7] has studied the structure of membrane-electrode-assembly (MEA) using high-resolution scanning electron microscopy (HR-SEM). In his investigation he has shown that the catalyst layer consists of a random distribution of pores and particles, see Fig. 1. It was also shown, using higher magnification, that the particles are agglomerates of much smaller particles coated with a film of Nafion. From the images in the figure it can be clearly seen that the agglomerates are spherical in shape. Lee et al. [8] and Liu et al. [9] have also published their investigations of PEM fuel cell electrodes using SEM/TEM that corroborate Middleman's work. Therefore, spherical

agglomerates can be treated as realistic representation of cathode catalyst layers in PEM fuel cells for modeling purposes. The utility of this conceptualization over macrohomogeneous characterization is clearly described during model validation, Section 5.

3. Steady state model

A schematic of the PEM fuel cell cathode that is modeled in this work is illustrated in Fig. 2. The schematic shows the bipolar plate at the top, Toray carbon paper (TGP 120) as a diffusion layer, microporous layer below that, and the catalyst layer at the bottom. The bipolar plate consists of straight channels of uniform cross-section. As air travels along the channels, it transports through the diffusion layer and microporous layer and enters the catalyst layer. Typically, fuel cell catalyst layer models are based on the assumption of either macrohomogeneous or flooded-agglomerate structure [21,45,49,51,54,58,59]. In this work, the catalyst layer has been modeled considering both the macrohomogeneous and the spherical flooded-agglomerate structure. For the case of PEM fuel cells, a flooded-agglomerate is a uniform mixture consisting of Pt nanoparticles supported on carbon with the hydrated ionomer in the micropores. Hence, the catalyst layer consists of a cluster of flooded-agglomerates with free space in between for the gas to diffuse through and reach the surface of each flooded-agglomerate. In addition, each spherical agglomerate is assumed to be coated with a thin film of ionomer. Fig. 3 shows the schematic of the catalyst layer and an enlarged view of the spherical agglomerate. The figure also shows the membrane layer below the catalyst layer. At the surface of the ionomer, oxygen present in the gas dissolves into the water present inside the pores of the ionomer. At the surface it is assumed that there exists an equilibrium between the partial pressure of oxygen in the gas phase and the dissolved concentration in the ionomer phase. The dissolved oxygen diffuses through the ionomer pores and reaches the active catalyst sites, where the following oxygen reduction reaction takes place:

$$O_2 + 4H^+ + 4e^- \rightarrow 2H_2O \quad (1)$$

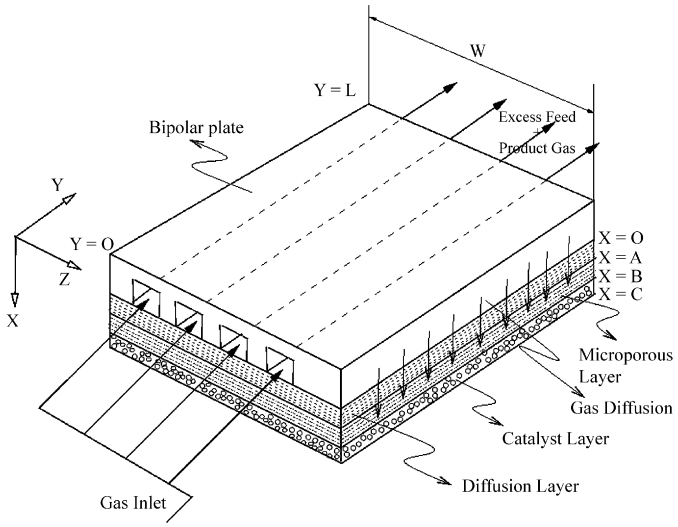

Fig. 2. Schematic of a PEM fuel cell cathode.

The hydrogen ions produced in the anode catalyst layer travel across the membrane layer and reach active catalyst sites inside the cathode through a network of micropores in the ionomer. Detailed model equations for the gas flow channel, diffusion layer, microporous layer and catalyst layer of the PEM fuel cell are described below. The reader is referred to the nomenclature for details on variables and parameters description. The following assumptions are considered for setting up the model equations:

Assumption 1. Isothermal conditions are considered throughout the region of interest.

Assumption 2. Pressure gradients in the X direction in all the regions are negligible. Hence, velocities in the X direction are zero.

Assumption 3. Effective diffusivities are assumed for diffusive transport in the gas phase inside the porous regions.

Assumption 4. Butler–Volmer kinetics are considered for the oxygen reduction reaction.

Assumption 5. Physical properties of the ionomer inside the catalyst layer are considered same as that of the membrane.

Assumption 6. Potential drop in the solid phase due to resistance to the electron transport is assumed to be negligible.

Assumption 7. The gas mixture inside the region of interest is assumed to behave as an ideal gas.

Even though some of the above assumptions are generally not valid for all cases, they have been considered for various reasons. The assumption of isothermal conditions was based on the fact that the unit cell considered for model validation was small, with an active area of 20 cm^2. For more detailed two-phase studies, it will be important to consider non-isothermal effects in the various regions of the fuel cell [39]. Meng and Wang [60] investigated the effects of electron transport through the gas diffusion layer (GDL) for the first time. They show that the current distribution was determined by two factors: oxygen supply and lateral electronic resistance in GDL. At a high cell voltage, the lateral electronic resistance dictated the current distribution and at low cell voltages, oxygen concentration played a dominant role in determining the current distribution. However, potential drop effects due to electron transport were assumed negligible in order to avoid making the model more complex and not to deviate from the main focus of the paper—to highlight the liquid water effects in the different regions of the fuel cell cathode.

3.1. Gas flow channel

The following assumptions are considered for the gas flow channels:

- All channels in the graphite plate are assumed to have equal air flow rate.
- Negligible edge effects. This would result in $u_z = 0$
- Based on the previous assumption,$u_x = 0$

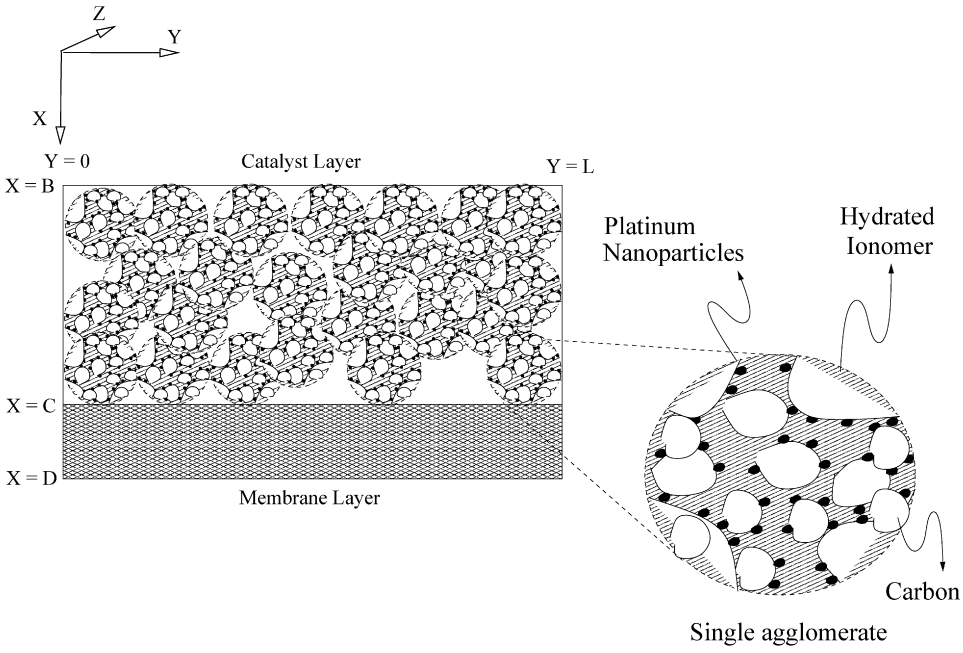

Fig. 3. Schematic of a PEM fuel cell catalyst layer and spherical agglomerate.

- The boundary condition of no slip at the walls has also been relaxed and a constant velocity in Y direction is assumed. This gives us

$$u_y = u_{\text{inlet}} \tag{2}$$

  This simplification has been made in spite of the existence of a fully developed velocity profile for rectangular ducts [61]
- The liquid water inside the gas flow channels is assumed to exist in the form of tiny droplets and travel with the gas velocity [62]. Hence, mist flow model is applied to describe liquid water transport in the gas flow channels

Hence, gas flow and liquid water transport in the channels can be considered as a plug flow with simultaneous exchange of species at the boundary between the gas flow channels and the backup substrate. A schematic of a control volume inside the gas flow channel is illustrated in Fig. 4.

The species molar balance equation inside the gas flow channels can be written as

$$-\frac{\partial}{\partial y}(C_{i,\text{gc}}u_{\text{inlet}}) - \nabla\cdot\mathbf{J}_i = 0 \tag{3}$$

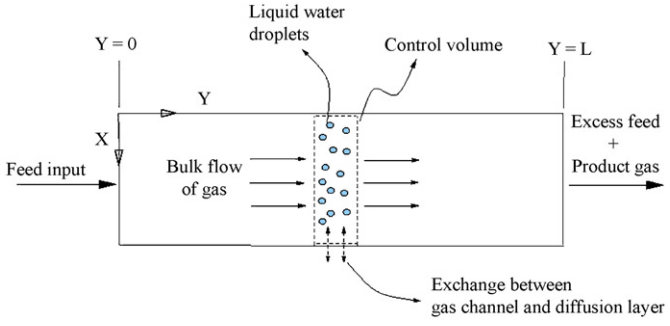

Fig. 4. Control volume inside gas flow channel.

where, $\mathbf{J}_i$ is the flux due to diffusion of species i into the diffusion layer from the gas flow channel. It is calculated from the local flux evaluated at the boundary $x = 0$ and can be expressed as

$$\mathbf{J}_i = -D_{i,\text{effd}}\nabla C_{i,\text{d}}|_{x=0} \tag{4}$$

where, $D_{i,\text{effd}}$ is the effective diffusivity of species i inside the diffusion layer and $C_{i,\text{d}}$ is the concentration of species i inside the diffusion layer.

For water vapor, an additional term accounting for evaporation/condensation appears in the above species balance equation. Hence, the conservation equation for water vapor can be written as

$$-\frac{\partial}{\partial y}(C_{\text{H}_2\text{O,gc}}u_{\text{inlet}}) - \nabla\cdot\mathbf{J}_{\text{H}_2\text{O}} - R_{\text{w}} = 0 \tag{5}$$

where R_{w} is the interfacial transfer of water between liquid and water vapor and is defined as [24]

$$R_{\text{w}} = k_{\text{c}}\frac{\epsilon_k(1-s)}{RT_{\text{cell}}}y_{\text{w}}(p_{\text{w}} - p_{\text{w}}^{\text{sat}})q + k_{\text{v}}\frac{\epsilon_k s\rho_{\text{w}}}{M_{\text{w}}}(p_{\text{w}} - p_{\text{w}}^{\text{sat}})(1-q) \tag{6}$$

where k_{c} and k_{v} are the condensation and evaporation rate constants, respectively; ϵ_k is the void fraction (= 1.0 for gas flow channel); s is the liquid water saturation level, which is the fraction of void volume occupied by liquid water; y_{w} and p_{w} are mole fraction and partial pressure of water vapor, respectively; and $p_{\text{w}}^{\text{sat}}$ is the water vapor saturation pressure. The parameter q is a switching function that is defined by [24]

$$q = \frac{1.0 + (|p_{\text{w}} - p_{\text{w}}^{\text{sat}}|)/(p_{\text{w}} - p_{\text{w}}^{\text{sat}})}{2} \tag{7}$$

Hence, if $p_{\text{w}} \geq p_{\text{w}}^{\text{sat}}$ then $q = 1$ and the interfacial transfer of water will be a condensation process. On the other hand, if $p_{\text{w}} <$

p_w^{sat} then $q = 0$ and the interfacial transfer of water will be an evaporation process.

The conservation for liquid water in the gas flow channel can be written as

$$-\frac{\rho_w}{M_w}\frac{\partial}{\partial y}(s_{gc}u_{inlet}) - \nabla\cdot\mathbf{N}_{w,d} + R_w = 0 \quad (8)$$

where s_{gc} is the fraction of volume occupied by the liquid water in the gas flow channel; $\mathbf{N}_{w,d}$ is the flux of liquid water into the gas flow channel from the diffusion layer. It is given by Darcy's law and is described in the next section.

3.2. Diffusion Layer

Since no pressure gradients are assumed inside diffusion layer, transport of species is governed purely by diffusion due to concentration gradients. Moreover, in order to simplify computations, diffusive transport is defined using Fick's law with an effective diffusivity instead of using Stefan–Maxwell equations. Recent numerical studies [63,64] have shown that Fick's formula with effective diffusion coefficient leads practically to the same results as those with Stefan–Maxwell equations. In the absence of any reaction in the diffusion layer, species conservation equations can be written as

$$-\nabla\cdot(-D_{i,effd}\nabla C_{i,d}) - R_w = 0 \quad (9)$$

where, $D_{i,effd}$ is the effective diffusivity and $C_{i,d}$ is the concentration of species i inside the diffusion layer. The effective diffusivities of species in porous regions are related to the diffusivities in gaseous regions by the equation

$$D_{i,eff} = \epsilon_k^{3/2}(1-s)^{3/2}D_{im} \quad (10)$$

where ϵ_k is the porosity of the region k, s is the liquid water saturation and D_{im} is the diffusivity of the species i in the mixture, which is related to the binary diffusivities and is given by [65]

$$D_{im} = (1-y_i)\left(\sum_{j=1;j\neq i}^{N}\frac{y_j}{D_{ij}}\right)^{-1} \quad (11)$$

The binary diffusion coefficients in the above equation are estimated using Chapman–Enskog formula [66]. The term R_w in Eq. (9) is applicable only for water vapor conservation, which defines the volumetric rate of evaporation/condensation and is given in Eq. (6).

In the porous regions (diffusion layer, microporous layer and catalyst layer), the liquid water is driven by capillary force. Darcy's law is used to describe the flow of liquid water

$$\mathbf{u}_l = -\frac{K_w(s)}{\mu_w}\nabla(P_l) \quad (12)$$

Therefore, the molar flux of liquid water can be written as

$$\mathbf{N}_w = -\frac{\rho_w K_w(s)}{M_w\mu_w}\nabla(P_l) \quad (13)$$

where ρ_w, M_w, and μ_w are density, molecular weight, and viscosity of liquid water, respectively; $K_w(s)$ is the permeability of liquid water in the porous regions. The capillary pressure is defined as the difference between total gas pressure (P_g) and pressure of liquid water (P_l)

$$P_c = P_g - P_l \quad (14)$$

Therefore, Eq. (13) can be written as

$$\mathbf{N}_w = -\frac{\rho_w K_w(s)}{M_w\mu_w}\nabla(P_g - P_c) \quad (15)$$

Since gas phase pressure gradients are assumed negligible inside porous regions, the above equation reduces to

$$\mathbf{N}_w = -\frac{\rho_w K_w(s)}{M_w\mu_w}\nabla(-P_c) \quad (16)$$

$$= -\frac{\rho_w K_w(s)}{M_w\mu_w}\left(-\frac{dP_c}{ds}\right)\nabla s \quad (17)$$

Both capillary pressure (P_c) and permeability ($K_w(s)$) are functions of liquid water saturation (s). Several empirical expressions are available to describe the dependence of P_c and $K_w(s)$ on the liquid water saturation [24,62]. In order to reduce the number of fitting parameters in the model, $(-dP_c/ds)$ is treated as a constant and $K_w(s)$ is assumed to depend linearly on liquid water saturation, i.e., $K_w(s) = K_{wo}s$, where K_{wo} is the permeability of liquid water at 100% saturation [53].

Writing a conservation equation for liquid water in the absence of any reaction in the diffusion layer leads to

$$-\nabla\cdot\mathbf{N}_w + R_w = 0 \quad (18)$$

3.3. Microporous layer

For modeling purposes, the microporous layer is similar to the diffusion layer. The only difference is in the physical parameters such as, the void fraction, pore structure and thickness. Hence, based on the same assumptions considered for writing species conservation equations for the diffusion layer, the conservation equations for species in gas phase and liquid water inside the microporous layer can be written as

$$-\nabla\cdot(-D_{i,effm}\nabla C_{i,m}) - R_w = 0 \quad (19)$$

$$-\nabla\cdot\mathbf{N}_w + R_w = 0 \quad (20)$$

where, $D_{i,effm}$ is the effective diffusivity and $C_{i,m}$ is the concentration of species i inside the microporous layer.

3.4. Catalyst layer

Based on the same assumptions for transport within diffusion layer and microporous layer, the conservation equation inside the catalyst layer for species i in the gas phase can be written as

$$-\nabla\cdot(-D_{i,effr}\nabla C_{i,r}) + R_i - R_w = 0 \quad (21)$$

where, $D_{i,effr}$ is the effective diffusivity and $C_{i,r}$ is the concentration of species i inside the catalyst layer. In Eq. (21), R_i represents the consumption of oxygen or production of water per unit volume of catalyst layer. Similar to the diffusion layer

and microporous layer, R_w in the above equation is applicable only for the water vapor balance. Butler–Volmer equation is used to define the rate of oxygen reduction reaction

$$R_{O_2} = -\frac{a_a i_a}{n_e F} \tag{22a}$$

$$= -\frac{a_a i_o}{n_e F}\frac{C_{O_2,mem}}{C^s_{O_2}} \exp(-\frac{\alpha \eta_r F}{RT_{cell}}) \tag{22b}$$

where $C_{O_2,mem}$ is the dissolved concentration of oxygen in the ionomer adjacent to the catalyst site; $C^s_{O_2}$ is the saturation concentration of oxygen inside ionomer. The local overpotential (η_r) appearing in the Butler–Volmer kinetics is defined by the following equation:

$$\eta_r = \Delta\phi(s,r) - \Delta\phi_e(s,r) \tag{23a}$$

$$= \{\phi_s - \phi_r\} - \{\phi_{e,s} - \phi_{e,r}\} \tag{23b}$$

where ϕ_s is the potential of the solid phase and ϕ_r is the ionomer potential adjacent to active catalyst site. The subscript e denotes equilibrium conditions. If standard hydrogen electrode (SHE) is treated as the reference electrode, then the solid phase potential $\phi_s = V_{cat}$ and $\Delta\phi_e(s,r) = V_{oc}$, open circuit potential. Therefore, the local overpotential (η_r) and the ionomer phase potential (ϕ_r) are related by the following equation

$$\eta_r = V_{cat} - \phi_r - V_{oc} \tag{24}$$

Now the question is: how does one determine the dissolved concentration of oxygen inside the ionomer at the active catalyst sites? To answer this question, the ideas of macrohomogeneous and spherical flooded agglomerate characterization for modeling the catalyst layer region are briefly described in the next two sections.

3.4.1. Macrohomogeneous characterization

Typically, catalyst layers in PEM fuel cells are prepared by synthesizing a uniform mixture of carbon coated with platinum nanoparticles and ionomer that is dissolved in a solvent. This uniform mixture is called the catalyst ink. A thin layer of catalyst ink is coated on to the membrane and dried. The solvent evaporates during drying, leaving a thin layer of catalyst coating that is usually in the range of 10–50 μm thick. Macrohomogeneous characterization assumes that any control volume inside the catalyst layer consists of a uniform mixture of platinum supported carbon and ionomer and voids. This is schematically represented in Fig. 5. Models based on macrohomogeneous structure assume that the concentration of oxygen in the ionomer phase is uniform throughout the mixture. Hence, $C_{O_2,mem}$ in Eq. (22b) is same as the concentration of oxygen inside the ionomer at the surface i.e.

$$C_{O_2,mem} = \frac{RT_{cell}}{H_{O_2,mem}} C_{O_2,r} \tag{25}$$

where $C_{O_2,r}$ is the concentration of oxygen in the voids inside the control volume; $H_{O_2,mem}$ is Henry's constant for oxygen between membrane and air. This assumption completely ignores the fact that the oxygen concentration will decrease from the surface to the active catalyst sites that are embedded inside the uniform mixture due to diffusion and reaction.

3.4.2. Spherical agglomerate characterization

Spherical agglomerate characterization assumes that the catalyst particles form agglomerates that are spherical in shape. Fig. 6 a shows the schematic of a single spherical agglomerate in isolation. A thin film of ionomer is also assumed on top of the agglomerate [8,7,9]. Another advantage with this characterization is that the water produced at the reaction sites can be conveniently accommodated using this model. A simple

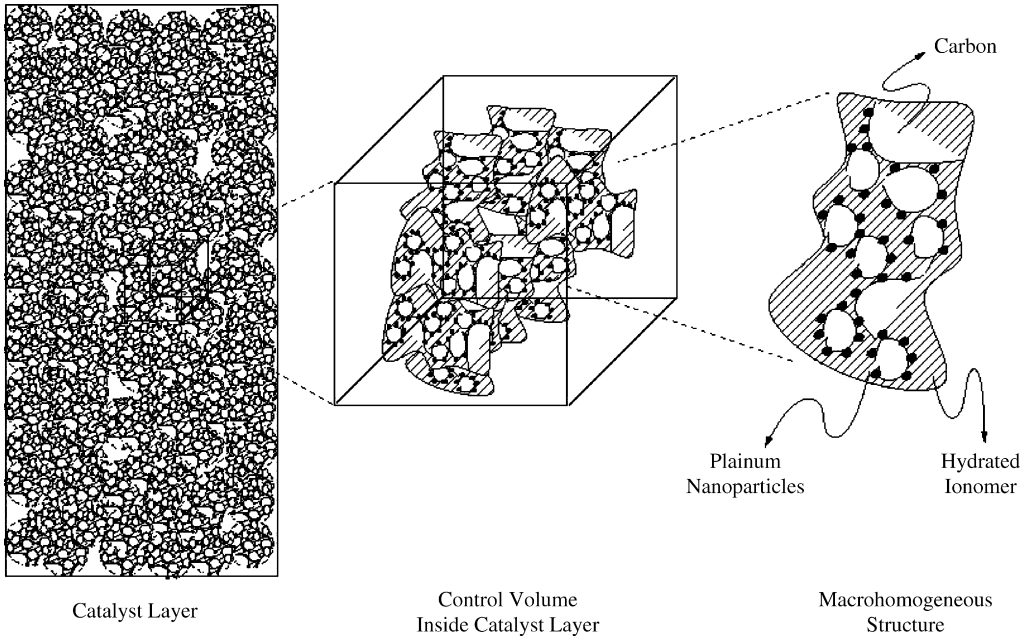

Fig. 5. Schematic of catalyst layer characterized using macrohomogeneous structure.

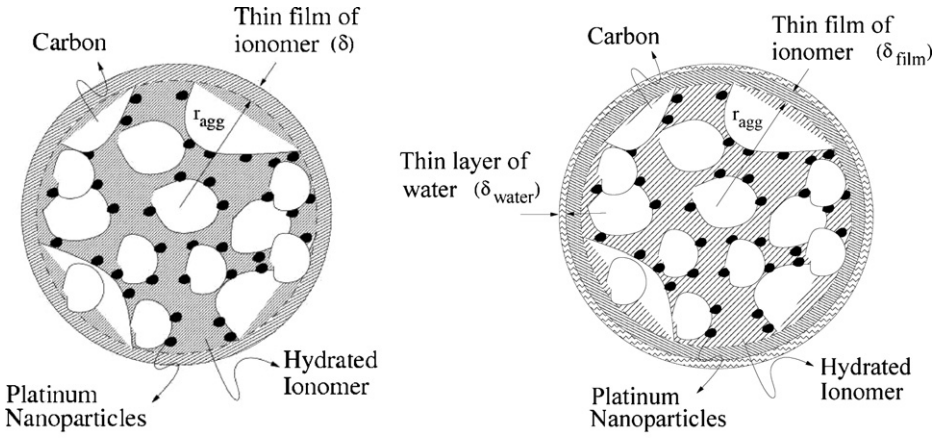

(a) With ionomer film (b) With ionomer film and water layer

Fig. 6. Spherical flooded-agglomerate for PEM fuel cells

approach is to assume that the water produced at the reaction sites diffuse to the surface of the agglomerate forming a thin film before participating in the evaporation/condensation process. A schematic of the spherical agglomerate with a thin film of water is shown in Fig. 6 b. The thickness of the water layer can be related to the local accumulation and could vary across the reaction layer.

Using spherical agglomerate characterization, one way to determine the volumetric rate of oxygen consumption inside the catalyst layer is to write species balance equations within a spherical agglomerate and solve for $C_{O_2,mem}$ as a function of agglomerate radius. Subsequently, the volumetric rate of oxygen consumption can be calculated based on the flux from the profile of oxygen concentration inside the ionomer or spherical agglomerate and the number density of spherical agglomerates within the catalyst layer. However, this method is very computationally intensive [67], as it requires solving for species balance equations within a spherical agglomerate for every control volume inside the catalyst layer. In order to reduce the time for computations, the method of Thiele modulus and effectiveness factor was adopted. Moreover, we have also assumed a linear profile for the concentration of dissolved oxygen inside the ionomer film. Even though the assumption of linear profile introduces some inaccuracy for calculating the flux, this particular method has been adopted earlier [53,68] and has been shown to be a good approximation for predictions. Lin et al. [5] characterized the catalyst layer through a cylindrical geometry and have used the Thiele modulus and effectiveness factor approach to calculate rate of oxygen reduction reaction. Sun et al. [68] have used the same approach for the catalyst layer characterized using spherical agglomerates with a thin film of ionomer. However, they have not considered any liquid water effects. The consumption of oxygen inside the catalyst layer can be written as

$$R_{O_2} = -\zeta k_{rxn} C_{O_2}|_{ns} \tag{26}$$

where k_{rxn} is the rate constant, given by

$$k_{rxn} = \frac{a_a i_o}{n_e F} \frac{1}{C^s_{O_2}} \exp\left(-\frac{\alpha \eta_r F}{RT}\right) \tag{27}$$

and ζ is defined as the effectiveness factor and for spherical geometry is given by [66]

$$\zeta = \frac{3}{\psi^2}(\psi \coth(\psi) - 1) \tag{28}$$

The Thiele modulus (ψ) in the above equation is given by

$$\psi = r_{agg}\sqrt{\frac{k_{rxn}}{D^{eff}_{O_2,mem}}} \tag{29}$$

where r_{agg} is the radius of agglomerate; $D^{eff}_{O_2,mem}$ is the effective diffusivity of oxygen in ionomer inside the spherical agglomerates. Concentration of oxygen appearing in Eq. (26) is at the ionomer and the spherical agglomerate interface and is given by

$$C_{O_2}|_{ns} = \frac{RT_{cell}/H_{O_2,mem} C_{O_2,r}}{\{1 + (\delta_{mem}/D_{O_2,mem})(1/a_1)\zeta k_{rxn}\}} \tag{30}$$

where δ_{mem} is the thickness of ionomer film; $D_{O_2,mem}$ is diffusivity of oxygen in ionomer film; a_1 is the surface area of agglomerate per unit volume of catalyst layer and is given by

$$a_1 = \frac{2(2\pi - 2\beta)(r_{agg} + \delta_{mem})^2 N_{agg}}{((4/3)\pi(r_{agg} + \delta_{mem})^3 N_{agg})/(1 - \epsilon_r)} = \frac{3}{(r_{agg} + \delta_{mem})}(1 - \frac{\beta}{\pi})(1 - \epsilon_r) \tag{31}$$

Here 2β is the angle covered by particles or membrane which is required for the flow of electrons and protons into the spherical agglomerate. The ratio β/π is the fraction of surface area unavailable for transport of gaseous components and liquid water. In the work of [68], the authors have considered only an electrolyte film covering the spherical agglomerate. They mention that a fraction of the agglomerate surface is occupied by electrolyte, but they have not tried to quantify the area required as pathways for proton transport. In the cylindrical agglomerate characterization of [53], a liquid water layer on the top of the nafion film has been considered. The authors have not considered the top and the bottom area of the cylinder for oxygen and liquid water transport. An experimental method might be

designed to determine such a ratio for a particular system. It may also be used as a fitting parameter in a model in absence of any experimental data. In order to reduce the number of fitting parameters in the model, β has been treated as zero in this study. A sensitivity study will be done in future to study the effect of this fraction on the model output. When liquid water forms a thin film on top of the spherical agglomerates, it provides additional resistance to the transport of oxygen. The additional resistance due to water can be accommodated into Eq. (30) by following the above analysis, which results in

$$C_{O_2}|_{ns} = \frac{(RT_{cell}/H_{O_2,mem})C_{O_2,r}}{1 + ((\delta_{mem}/a_1 D_{O_2,mem}) + (\delta_w/a_1 D_{O_2,w})(H_{O_2,w}/H_{O_2,mem}))\zeta k_{rxn}} \quad (32)$$

where δ_w is thickness of the water layer; $D_{O_2,w}$ is diffusivity of oxygen in liquid water; $H_{O_2,w}$ is Henry's constant for oxygen between liquid water and air. The thickness of water layer is given by

$$\delta_w \approx \frac{\epsilon_r s_r}{a_1} \quad (33)$$

From the stoichiometry of the overall reaction, amount of water produced in the cathode catalyst layer is twice the amount of oxygen consumed. Hence, conservation equation for liquid water can be written as

$$-\nabla \cdot \mathbf{N}_w - 2R_{O_2} + R_w = 0 \quad (34)$$

Hydrogen ions produced at the anode catalyst layer travel through the membrane and reach the active catalyst sites in the cathode catalyst layer. Writing the charge conservation equation over a small volume element inside the catalyst layer leads to,

$$-\nabla \cdot \mathbf{j}_r + n_e F R_{O_2} = 0 \quad (35)$$

where $\mathbf{j}_r$ is the local current density inside the cathode catalyst layer. For describing the transport of hydrogen ions inside the ionomer network, Ohm's law with an effective ionomer conductivity and ionomer potential gradient is considered. Hence, local current density for the same control volume element can be written as

$$\mathbf{j}_r = -\kappa_{eff} \nabla \phi_r \quad (36)$$

where κ_{eff} is the effective conductivity of ionomer inside the catalyst layer. It is related to the fraction of volume occupied by ionomer (ϵ_{mem}) inside catalyst layer and ionomer conductivity (κ_{mem}) by the following equation [5]:

$$\kappa_{eff} = \epsilon_{mem}^{3/2} \kappa_{mem} \quad (37)$$

Substituting the Ohm's law in Eq. (35) leads to

$$\epsilon_{mem}^{3/2} \kappa_{mem} \nabla^2 \phi_r + nFR_{O_2} = 0 \quad (38)$$

The cell current density (i_{cell}) is calculated by integrating the hydrogen ion flux at the cathode catalyst layer and membrane interface. It can expressed as

$$i_{cell} = \frac{1}{w_{cell} L} \int_{y=0}^{y=L} \left\{ -\epsilon_{mem}^{3/2} \kappa_{mem} \frac{\partial \phi_r}{\partial x}|_{x=C} \right\} w_{cell} \, dy \quad (39)$$

3.4.3. Expressions for ϵ_r, ϵ_{mem} and δ_{mem}

As mentioned in the introduction, the spherical agglomerate characterization is used in deriving the expressions for ϵ_{mem}, ϵ_r and δ_{mem} as a function of the physical and experimental parameters of the catalyst layer such as the thickness (t_{RL}) and area (a_{RL}) of the catalyst layer, weight fraction of platinum on carbon (f_{pt}), catalyst loading (m_{pt}), and the weight fraction of the ionomer (f_{mem}). The fraction of volume occupied by the voids inside the catalyst layer is defined by the following equation:

$$\epsilon_r = \frac{v_v}{v_{RL}} \quad (40a)$$

$$= 1.0 - \frac{v_s}{v_{RL}} \quad (40b)$$

The volume of the solids inside the catalyst layer can be defined as the total sum of the volumes of carbon, platinum and ionomer. Hence,

$$v_s = v_c + v_{pt} + v_{mem} \quad (41)$$

Writing the volumes of carbon, platinum and ionomer in terms of their mass and density give us

$$v_s = \frac{w_c}{\rho_c} + \frac{w_{pt}}{\rho_{pt}} + \frac{w_{mem}}{\rho_{mem}} \quad (42)$$

The following definitions are used for the weight fractions of platinum and ionomer

$$f_{pt} = \frac{w_{pt}}{w_{pt} + w_c} \quad (43a)$$

$$f_{mem} = \frac{w_{mem}}{w_{pt} + w_c + w_{mem}} \quad (43b)$$

Solving Eqs. (43a) and (43b) for w_c and w_{mem}, respectively and substituting in Eq. (42) leads to

$$v_s = \frac{w_{pt}}{f_{pt}} \left\{ \frac{f_{pt}}{\rho_{pt}} + \frac{1 - f_{pt}}{\rho_c} + \frac{f_{mem}}{(1 - f_{mem})\rho_{mem}} \right\} \quad (44)$$

The volume of the catalyst layer (v_{RL}) in Eq. (40b) is the product of its cross-sectional area (a_{RL}) and thickness (t_{RL}). Substituting for v_s and v_{RL} in Eq. (40b) gives

$$\epsilon_r = 1.0 - \frac{1}{f_{pt}} \left\{ \frac{f_{pt}}{\rho_{pt}} + \frac{1 - f_{pt}}{\rho_c} + \frac{f_{mem}}{(1 - f_{mem})\rho_{mem}} \right\} \frac{w_{pt}}{a_{RL} t_{RL}} \quad (45a)$$

$$= 1.0 - \frac{1}{f_{pt}} \left\{ \frac{f_{pt}}{\rho_{pt}} + \frac{1 - f_{pt}}{\rho_c} + \frac{f_{mem}}{(1 - f_{mem})\rho_{mem}} \right\} \frac{m_{pt}}{t_{RL}} \quad (45b)$$

The fraction of volume occupied by ionomer inside the catalyst layer is given by

$$\epsilon_{mem} = \frac{v_{mem}}{v_{RL}} \quad (46a)$$

$$= \frac{1}{v_{RL}} \frac{w_{mem}}{\rho_{mem}} \quad (46b)$$

Solving for w_{mem} using Eqs. (43a) and (43b) and substituting in Eq. (46b) leads to

$$\epsilon_{mem} = \frac{1}{v_{RL}\rho_{mem}} \left\{ \frac{f_{mem}}{1.0 - f_{mem}} \right\} \frac{w_{pt}}{f_{pt}} \quad (47a)$$

$$= \frac{1}{t_{RL}\rho_{mem}} \left\{ \frac{f_{mem}}{1.0 - f_{mem}} \right\} \frac{m_{pt}}{f_{pt}} \quad (47b)$$

Based on a mass balance on Nafion, it can be shown that

$$\delta_{mem} = \frac{r_{agg}}{3\rho_{mem}} \frac{(f_{mem}/1 - f_{mem})(1 - (1/\rho_{mem}))}{(f_{pt}/\rho_{pt}) + (1 - f_{pt}/\rho_c) + (f_{mem}(1 - f_{mem})\rho_{mem})} \quad (48)$$

3.5. Boundary conditions, other relationships and dimensionality

The constitutive relationships and other equations defining some of the parameters appearing in the above equations are given in Table 1. The boundary conditions for different sections of the cathode are given in Table 2. Gas entering at the cathode inlet is assumed to be a mixture of air and water vapor with no liquid water saturation (BC1). At the boundaries of the gas flow channel/Diffusion layer, diffusion layer/microporous layer, microporous layer/catalyst layer, continuity of the variables and flux continuity are imposed. Boundary conditions 2 and 3 suggest that the liquid water saturation is continuous at the gas flow channel/diffusion layer and the liquid water flux is also equal.

The boundary conditions for the liquid water saturation (s) need a detailed discussion in this context. The conservation equation for liquid water in gas flow channel is first order in y. We have considered the inlet saturation of gas as the boundary condition for this equation. The conservation equations for liquid water in the gas diffusion layer (GDL), microporous layer (MPL) and catalyst layer (CL) are second order in x. The obvious and well accepted boundary conditions are continuity of flux at CL/MPL interface and MPL/GDL interface. No flux condition is assumed at CL/membrane interface. But three more boundary conditions are required—each at channel/GDL interface, GDL/MPL interface and at MPL/CL interface.

A survey of the published literature reflect the different boundary conditions adopted by different authors. Pasaogullari and Wang [4] considers the catalyst layer to be ultrathin and therefore the oxygen reduction reaction is assumed to take place at the interface of PEM and diffusion layer. Therefore, only the continuity of flux is used as a boundary condition at this interface. In their work, they assume the liquid saturation at the channel/GDL interface to be zero. In another work by [44], the same boundary conditions as above have been considered. In the work of [24], the flux of liquid water at channel/GDL interface has been considered zero at the inlet. At the outlet, the authors have considered $\partial s/\partial y = 0$ as a boundary condition. The authors have also considered the catalyst layer to be ultrathin. Therefore the single boundary condition of continuity of flux is sufficient for them at GDL/membrane interface. Natarajan and Nguyen [69] assume that once the gas stream in the gas flow channel is saturated, the boundary conditions of liquid water saturation for subsequent volume elements at channel/GDL interface become 0.1. In that work, they have considered reaction layer as ultrathin requiring only the flux boundary condition. In the work of [53],

Table 1
Constitutive relations

Parameter	Expression	Reference
$D_{i,eff}$	$\epsilon_k^{3/2}(1-s)^{3/2}D_{im}$	Bruggeman relation
$K_w(s)$	$K_{wo}s$	[53]
a_a	$\frac{m_{pt}a_{pt}}{t_{RL}}$	
$C^s_{O_2}$	$\frac{1.0}{H_{O_2,mem}}$	
$H_{O_2,mem}$	$1.33\exp\left(-\frac{666.0}{T_{cell}}\right)$	[11]
$H_{O_2,w}$	$5.08\exp\left(-\frac{498.0}{T_{cell}}\right)$	[72]
$D_{O_2,mem}$	$3.1\times10^{-7}\exp\left(-\frac{2768}{T_{cell}}\right)$	[73,11]
$D^{eff}_{O_2,mem}$	$\epsilon_{mem}^{3/2}D_{O_2,mem}$	Bruggeman relation
κ_{mem}	$100.0(0.005139\lambda_w - 0.00326)\exp\left[1268.0\left(\frac{1}{303.0} - \frac{1}{T_{cell}}\right)\right]$	[36]
λ_w	$0.043 + 17.81a_w - 39.85a_w^2 + 36.0a_w^3$ for $0 < a_w \le 1$, $14.0 + 1.4(a_w - 1)$ for $1 \le a_w \le 3$, 16.8 for $a_w > 3$	[36]
a_w	$\frac{p_{w,r}}{p^{sat}_w}$	
p^{sat}_w	$\frac{1.02}{1000}(T)^{-4.9283}10^{(23.5518-(2937.8/T))}$	
ρ_{mem}	$\left(\frac{1.98 + 0.0324\lambda_w}{1 + 0.0648\lambda_w}\right)\times10^3$	[74]

Table 2
Boundary conditions for PEM fuel cell cathode shown in Fig. 2

Number	Location	Boundary condition	Comments
Gas flow channel			
BC1	$Y = 0$	$C_i = C_{io}$, $s_{gc} = 0$	$i = O_2, N_2, H_2O$, liquid saturation at inlet
Diffusion layer			
BC2	$X = 0, \forall Y$	$C_{i,d} = C_{i,gc}$, $s_{gc} = K_1 s_d$	Continuity at surface
BC3	$X = A, \forall Y$	$-D_{i,effm}\frac{\partial C_{i,m}}{\partial x} = -D_{i,effd}\frac{\partial C_{i,d}}{\partial x}$, $N_{w,m}\|_x = N_{w,d}\|_x$	Flux continuity in X direction
BC4	$0 < X \le A, Y = 0$	$-D_{i,effd}\frac{\partial C_{i,d}}{\partial y} = 0$, $N_{w,d}\|_y = 0$	Zero flux condition in Y direction
BC5	$0 < X \le A, Y = L$	$-D_{i,effd}\frac{\partial C_{i,d}}{\partial y} = 0$, $N_{w,d}\|_y = 0$	Zero flux condition in Y direction
Microporous layer			
BC6	$X = A, \forall Y$	$C_{i,d} = C_{i,m}$, $s_d = K_2 s_m$	Continuity at surface
BC7	$X = B, \forall Y$	$-D_{i,effm}\frac{\partial C_{i,m}}{\partial x} = -D_{i,effr}\frac{\partial C_{i,r}}{\partial x}$, $N_{w,m}\|_x = N_{w,r}\|_x$	Flux continuity in X direction
BC8	$A < X \le B, Y = 0$	$-D_{i,effm}\frac{\partial C_{i,m}}{\partial y} = 0$, $N_{w,m}\|_y = 0$	Zero flux condition in Y direction
BC9	$A < X \le B, Y = L$	$-D_{i,effm}\frac{\partial C_{i,m}}{\partial y} = 0$, $N_{w,m}\|_y = 0$	Zero flux condition in Y direction
Catalyst layer			
BC10	$X = B, \forall Y$	$C_{i,r} = C_{i,m}$, $s_m = K_3 s_r$, $-\epsilon_{mem}^{3/2}\kappa_{mem}\frac{\partial \phi_r}{\partial x} = 0$	Continuity at surface in X direction, zero flux for H^+ ions
BC11	$X = C, \forall Y$	$-D_{i,effr}\frac{\partial C_{i,r}}{\partial x} = 0$, $N_{w,r}\|_x = 0$, $\phi_r = 0$	Zero flux condition in X direction, reference point
BC12	$B < X \le C, Y = 0$	$-D_{i,effr}\frac{\partial C_{i,r}}{\partial y} = 0$, $N_{w,r}\|_y = 0$, $-\epsilon_{mem}^{3/2}\kappa_{mem}\frac{\partial \phi_r}{\partial y} = 0$	Zero flux condition in Y direction, zero flux for H^+ ions
BC13	$B < X \le C, Y = L$	$-D_{i,effr}\frac{\partial C_{i,r}}{\partial y} = 0$, $N_{w,r}\|_y = 0$, $-\epsilon_{mem}^{3/2}\kappa_{mem}\frac{\partial \phi_r}{\partial y} = 0$	Zero flux condition in Y direction, zero flux for H^+ ions

the transport of liquid water in the gas flow channel is not considered in their one-dimensional model. The liquid water saturation is considered to be same at the inlet and along the channel. In this model, liquid water in the reaction layer has been modeled. The liquid water conservation equation in the GDL and CL is second order in s. But only one boundary condition is mentioned in their work.

In the subsequent work of [70], the same boundary conditions as before have been considered. The boundary condition that may be used at these various interfaces are the relation between interface saturations. But the interface saturation is a very complicated function of the surface properties and the operating conditions. One of the most comprehensive discussions about the interface saturation is first given by [30]. The authors expressed the interfacial saturation at channel/GDL interface as a function of channel gas velocity, contact angle and local current density. Although liquid water generation is related to the local current density, interfacial transfer of liquid water to vapor phase has been considered in the present model. Therefore a part of the liquid water gets transferred to vapor phase as it flows across the reaction layer, microporous layer and the diffusion layer to the flow channel. As long as the saturation pressure of water at the operating condition is not exceeded, the liquid water that has been transferred to vapor phase remains in vapor phase. Therefore it is unlikely that it should affect the saturation at the interface. So in the view of the authors:

$$\text{at } X = 0, \forall Y \quad S_{gc} = f_1(S_d, \theta, u_y) \tag{49}$$

A detailed experimental test is required to determine such a function for a particular system. A detailed procedure can be found in the work of [71]. In this model, for simplicity , a linear relationship between S_{gc} and S_d is assumed

$$\text{at } X = 0, \forall Y \quad S_{gc} = K_1 S_d \tag{50}$$

where K_1 is a constant. The constant is always less than one and might be used in either side of the equation to maintain the saturation s (which is a volume fraction) to be less than one. Similarly the saturation at the GDL/MPL interface will depend on the wettability of both the surfaces. So

$$\text{at } X = A, \forall Y \quad S_{bs} = f_2(S_m, \theta_1, \theta_2) \tag{51}$$

where θ_1 and θ_2 are the contact angles of backup substrate and the diffusion layer respectively. If the medium is hydrophilic, $\theta \le 90^\circ$ whereas for a hydrophobic medium, $\theta > 90^\circ$. The velocity of gas in the porous media may also affect the interface saturation. In this work, the gas phase velocity has been considered negligible. In the absence of any experimental data, and for simplicity, here also a linear relationship between S_d and

S_m is assumed:

$$\text{at } X = A, \forall Y \quad S_{bs} = K_2 S_m \tag{52}$$

K_2 is a constant in Eq. (52). Because of similar reasons, one of the boundary conditions at the MPL/CL interface has been taken as:

$$\text{at } X = B, \forall Y \quad S_d = K_3 S_r \tag{53}$$

K_3 is a constant here. In this context, it may be mentioned that as (dP_c/ds) has been assumed constant in this study, the dependence of P_c on liquid saturation at different contact angles has not been explicitly modeled. The dependence has rather been assumed constant in this operating range and for the given surface wettabilities. Although the model does not consider the effect of varying hydrophobicity on the interphase saturation, the use of different constant values for different layers improves the predictive capability of the model significantly.

Fig. 2 depicts the geometry of the gas supply by using a machined graphite plate with straight flow channels. As we can see that the channels are separated by ribs or shoulders, which occlude half the flow area on top of the backup substrate. This necessitates considering flux variation in all the three directions (X, Y and Z) inside the porous regions. The ribbed geometry of the graphite plate causes the local flux to increase and causes a greater concentration drop than for a uniform flow. The idea of considering a uniform flow with a thicker diffusion layer that drops the concentration to an equivalent amount was expressed by [75]. They compared different geometries with various flux and concentration profiles for both steady state and dynamic cases and suggested an increase in the thickness of the diffusion layer by a factor of 0.6. In order to reduce the dimensionality in the steady and the subsequent dynamic models, the thickness of the diffusion layer has been increased by a factor of 0.6. Hence, in the steady state and the dynamic models, spatial variations are considered only in the Y direction inside the gas flow channel and in X and Y directions inside the porous regions.

4. Modeling methodology

The steady state model described in the previous section can be solved in two different ways. One method is to solve the model equations by considering cathode voltage, design and other model parameters as inputs and predict the cell current or current density. The second method is to treat the cell current or current density along with the design and model parameters as inputs and predict the cathode voltage. If we study the model equations carefully, we can see that the voltage appears inside an exponential term. Hence, it may be computationally less expensive to solve the model using the first method, i.e., treat voltage as an input and predict the current density. Preliminary trials in solving the model equations using both methods confirmed this point.

The model equations are essentially partial differential equations that are non-linear due to the interactions between the different variables. Since it may not be possible to obtain an analytical solution, the system of equations have been solved numerically. The next section describes in detail the methodology that was adopted for modeling and solving the system of equations.

4.1. Model development

The model development was carried out using Maple and subsequently, MATLAB was used to solve and simulate the model. The partial differential equations (PDEs) and the boundary conditions corresponding to the steady state model are setup in Maple in a symbolic manner. They are discretized in spatial variables using finite difference techniques and converted into a system of non-linear algebraic equations (NAEs). The discretization was done using an in-built Maple library function called convert and a Maple procedure, which can be used to produce finite difference approximations for PDEs. The procedure takes an expression and specifications for making finite difference approximations such as, backward, forward, or central difference formulae and the desired order as inputs. The output from the procedure is an expression representing the finite difference formula with appropriate indices. Hence, the PDEs and boundary conditions are converted to a list of NAEs in Maple. Further, the list of NAEs is converted into a procedure in Maple using an in-built library function called *proc*. Using a code generation package in Maple, the Maple procedure is converted into a MATLAB function, which essentially consists of all the equations. Finally, the MATLAB function can be called by an equation solver by passing appropriate parameters. In the present case, the non-linear algebraic equations are solved using *fsolve*, which is a part of MATLAB′s optimization toolbox. The whole procedure is schematically represented in Fig. 7.

4.2. Computational issues

Typically, there are several computational issues that are encountered while solving systems of PDEs and NAEs. Some of the issues and the techniques that have been used and/or developed to overcome them are highlighted below:

- Scaling of variables: several trials in solving the steady state and dynamic model equations demonstrated that the scaling of the variables is important due to the existence of highly non-linear terms in the equations. In its unscaled form, the system of equations could not be solved for the whole range of operating voltage. Hence, the variables in the equations have been appropriately scaled using the inlet conditions as reference values.
- Calculation of Jacobian: During preliminary trials in solving the model equations, it was observed that the numerical calculation of Jacobian was computationally very expensive. To overcome this, analytical expressions of non-zero elements in the Jacobian matrix were generated in Maple. These expressions were subsequently used by the solver *fsolve* while solving the system of equations. The use of analytical Jacobian greatly reduced the computational effort.

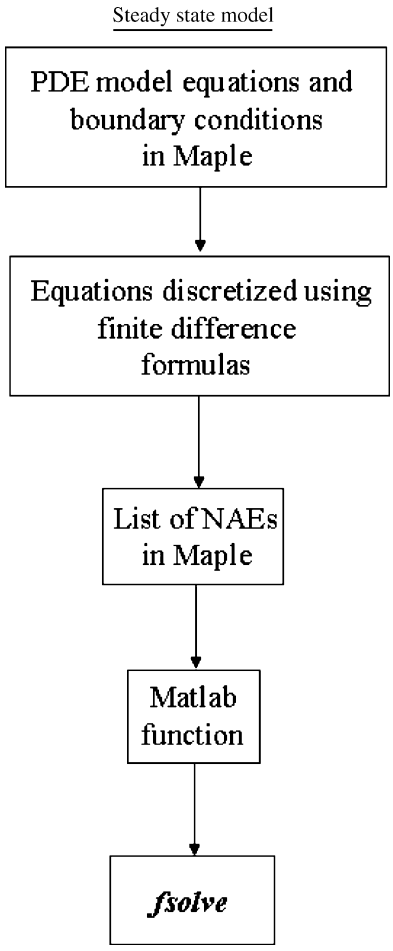

Fig. 7. Flowchart for modeling methodology.

- Grid sensitivity: Another important issue that has been studied is the sensitivity of the model predictions to the number of grids considered for writing the finite difference formulae. Different number of grids were considered in the *Y* direction in gas flow channel (GC), both the *X* and *Y* directions in diffusion layer, the microporous layer and the catalyst layer (RL). The steady state model was simulated and the sensitivity of the *i–v* curves is illustrated in Fig. 8. Based on this an appropriate number of grid points were chosen.

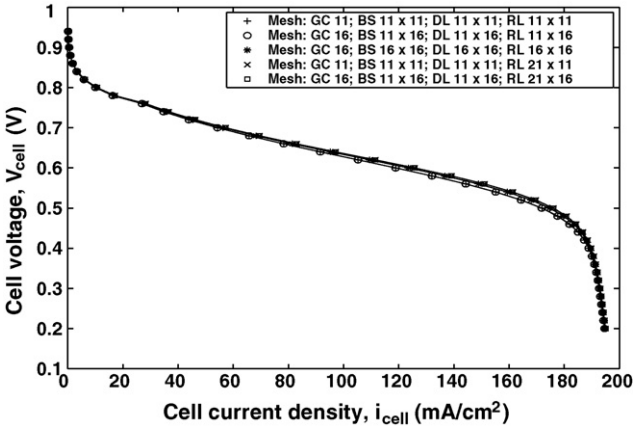

Fig. 8. Steady state polarization curves *vs.* mesh density.

5. Steady state model validation

Experimental data (*i–v* curves) for a PEM fuel cell was used to validate the steady state model. It was shown by [76] that experimental validation of multiphysics PEFC models must be done against data at the distribution level. However, for the scope of this study, the steady state model is validated using the overall *i–v* curves. Further validation of these models with distributed data is currently under progress.

The geometry of the PEM fuel cell is similar to that illustrated in Fig. 2. The cell consists of eight straight channels in the graphite plate and an effective MEA area of about 20 cm^2. The cell is operated at 65 °C. The design and other input parameters associated with the experimental data are given in Table 3. The fuel cell was operated with three different air flow rates. For every flow rate, the cell characteristic data was generated by operating the cell at different currents in the range of 0–10 A. Cathode voltage measured against standard hydrogen electrode (SHE) was recorded for each operating current. The steady state polarization data for the three different air flow rates are shown in Fig. 9. The data is an average of three different runs for every one of the flow rates. The next section describes about how the model described in Section 3 was validated against the experimental data represented in the above figure.

5.1. Model validation

As one can see from the description given in Section 3, various assumptions were introduced for writing the model equations. The validity of the assumptions are verified by comparing the corresponding simulation with the experimental data. The following modeling assumptions were tested: (i) transport

Table 3
Inputs and design parameters for experimental data

Parameter	Base case value	Units	Comments/reference
Inputs			
P_{cat}	≈ 1.0	atm	
F_{air}	0.2, 1.5 and 2.0	lpm	
V_{cat}	0.95 to 0.25	V	
T_{cell}	338.15	K	
T_{air}	343.15	K	
RH_{air}	100.0	%	
Design parameters			
w_{ch}	0.002	m	
h_{ch}	0.002	m	
L	0.07	m	
t_{GDL}	$350.0/0.6 \times 10^{-6}$	m	
t_{MPL}	450.0×10^{-6}	m	
t_{RL}	45.0×10^{-6}	m	
n_{ch}	8		
w_{cell}	0.03	m	
m_{pt}	0.2	mg Pt $cm^{-2}RL^{-1}$	
a_{pt}	20	m^2 Pt g^{-1} Pt^{-1}	
f_{pt}	0.20		
f_{mem}	0.25		
ϵ_{bs}	0.70		
ϵ_{d}	0.50		
ϵ_{r}	0.50		

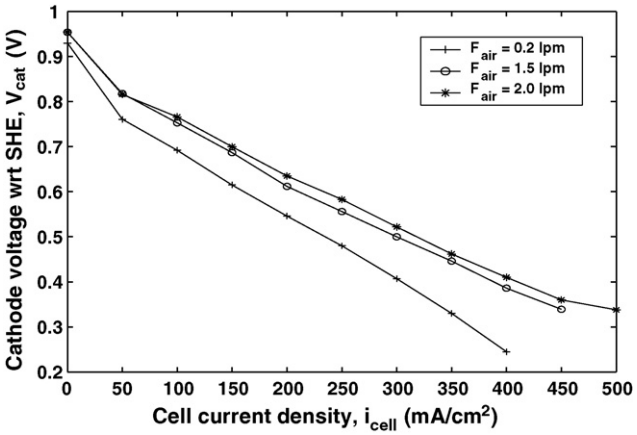

Fig. 9. Steady state polarization data for PEMFC cathode.

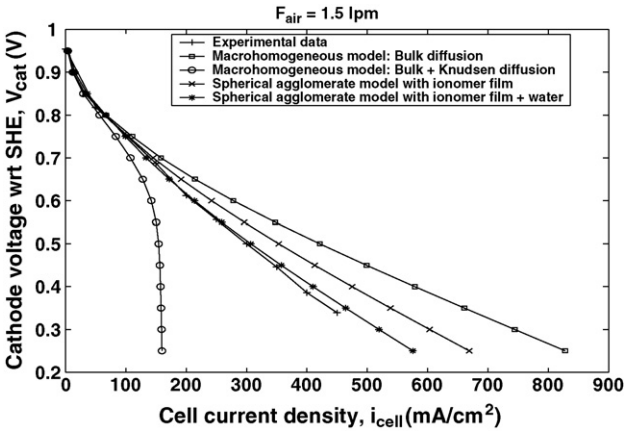

Fig. 10. Model predictions *vs.* experimental data. $F_{air} = 1.5$ lpm.

governed by diffusion in the bulk inside the porous regions (diffusion layer, microporous layer and catalyst layer), (ii) transport governed by simultaneous bulk and Knudsen diffusion, (iii) cathode catalyst layer characterized using a macrohomogeneous structure, (iv) cathode catalyst layer characterized using a spherical agglomerate structure, with and without liquid water effects. Various models, each representing the above assumptions were developed using the methodology described in Section 4. For model validation, the following procedure was adopted. The steady state experimental *i–v* data corresponding to $F_{air} = 1.5$ lpm was used to compare and tune the model predictions. The base case model parameters used for predicting the steady state polarization curve are listed in Table 4.

Fig. 10 shows the model predictions against the experimental data for the case where the cathode inlet air flow rate was 1.5 lpm. First, a macrohomogeneous model was used with the assumption that the transport in the porous regions take place only due to diffusion in bulk. The predicted *i–v* is shown using 'square' legend. It can be observed that the model prediction matches experimental data only in a small range of voltage, 0.95–0.75 V. Below 0.75 V, model predictions of current density are much higher than the experimental values. On the other hand, considering Kundsen and bulk diffusion in parallel, current density values predicted by the model (shown in open circles) are much less than the experimental values. Model studies where transport in the porous regions was assumed to be purely due to Kundsen diffusion were also studied and the predicted current density values were found be lower than experimental values. At the end of this exercise, it was concluded that transport in porous regions must be predominantly occurring due to diffusion in

Table 4
Model parameters for the base case

Parameter	Base case value (final value)	Units	Comments/reference
Model constants			
F	96485.3	$C\,g^{-1}eq.$	
n_e	4		
R	8.314	$J\,g^{-1}\,mol^{-1}\,K^{-1}$	
ρ_c	1.8×10^3	$kg\,m^{-3}$	
ρ_{pt}	21.45×10^3	$kg\,m^{-3}$	
ρ_w	983.21	$kg\,m^{-3}$	
Model parameters			
r_{agg}	1×10^{-7}	m	Middleman [7]
i_o	3.72×10^{-5} (3.84×10^{-3}) if $V_{cell} \geq 0.79$ V	$A\,m^{-2}\,Pt^{-1}$	Parthasarathy et al. [77]
	1.1×10^{-2} (3.2×10^{-1}) if $V_{cell} < 0.79$ V	$A\,m^{-2}\,Pt^{-1}$	Tuning parameter
α	1.0 if $V_{cell} \geq 0.79$ V		Parthasarathy et al. [77]
	0.625 if $V_{cell} < 0.79$ V		
k_c	100.0	s^{-1}	For all layers [53]
k_v	100.0	$atm^{-1}\,s^{-1}$	For all layers [53]
K_{wo}	7×10^{-15}	m^2	Catalyst layer [53]
	7×10^{-13}	m^2	Microporous layer [53]
	7×10^{-13} (1×10^{-10})	m^2	Diffusion layer (tuning parameter)
K_1	1.0		
K_2	1.0		
K_3	1.0		
$(-dP_c/ds)$	113.68	$N\,m^{-2}$	Catalyst layer [53]
	56.84	$N\,m^{-2}$	Microporous layer [53]
	56.84 (28.42)	$N\,m^{-2}$	Diffusion layer (tuning parameter)

the bulk. Hence, all subsequent models considered only bulk diffusion.

Next, a cathode model in which the catalyst layer was characterized using spherical agglomerate structure was simulated to predict the *i–v* data. The radius of the agglomerate considered for the model is shown in Table 4. In this model, it was assumed that all the water that is produced inside the cathode catalyst layer is in vapor form. The corresponding *i–v* data is shown using "×" legend in Fig. 10. It can be observed that even though the predicted current density values are higher than experimental data, they are significantly lower than the corresponding values predicted by the macrohomogeneous model. Subsequently, the spherical agglomerate model was extended to include the effects of liquid water in the porous regions, as described in Section 3. With liquid water effects, the model predictions matched very well with experimental data, as shown by the curve using "*" as legend. The match between experimental data and model prediction is clearly shown in Fig. 11.

Hence, it can be seen that when the catalyst layer is characterized with spherical agglomerates and transport in porous regions is by diffusion in bulk, the model predictions match very well with experimental data. The macrohomogeneous model assumes that within a small control volume in the catalyst layer, the dissolved concentration of oxygen is uniform throughout the homogeneous mixture of ionomer and platinum supported carbon. However, in the model based on spherical agglomerates, the dissolved concentration decreases from the surface of the ionomer to the active catalyst sites. Table 4 shows some of the model parameters that were used as tuning parameters. The final values of the tuning parameters are shown in parentheses in the table.

To check the validity of the model, experimental data corresponding to two very different air flow rates of 0.2 lpm (low) and 2.0 lpm (high) were compared to the model predictions. The results are shown in Figs. 12 and 13, respectively. It can be seen that the model predictions are close to the experimental data. Hence, with the given set of experimental data it can be concluded that the cathode model predictions are valid to a large extent with small deviations in some range of the operating voltage. Some of the assumptions that were made in Section 3

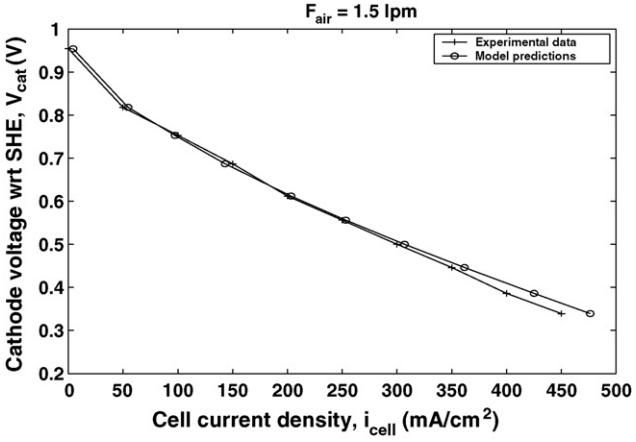

Fig. 11. Spherical agglomerate model predictions *vs.* experimental data. F_{air} = 1.5 lpm.

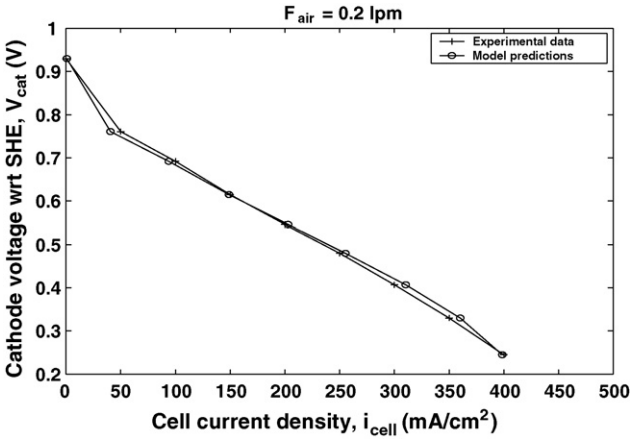

Fig. 12. Model predictions *vs.* experiment. F_{air} = 0.2 lpm.

for transport inside the gas flow channel and the porous regions were motivated by the cell design for which the experimental data was collected. The proposed cathode model has good predictive capabilities for small scale PEM fuel cells. The predictions of the proposed model needs to be tested against larger fuel cell designs.

Depending on the wettabilities of the materials at the different layers and operating conditions of the cell, the liquid water saturation at the interphases may vary widely. Meng and Wang [30] performed a sensitivity study on the value of the parameter that they use in their study at the channel/GDL interface. The authors have considered two values of the parameter at the channel/GDL interphase and have observed how a decrease in the interfacial liquid saturation improves the cell performance. In the present work, we have observed the effect of the interfacial saturation at MPL/CL interface on the cell performance. Fig. 14 shows that as K_3 varies from 1.0 to 0.4, the performance of the cell does not change much. As the value of K_3 decreases further, the cell reaches its limiting current density at a higher cell voltage than before. At a value of 0.2, the cell current density gets limited to about 200 mA/cm^2. As the value of K_3 gets reduced, the outflow of the liquid water from the cell gets reduced because of the reduced driving force. In other words, as the saturation level in the catalyst layer increases, the thickness of the water film

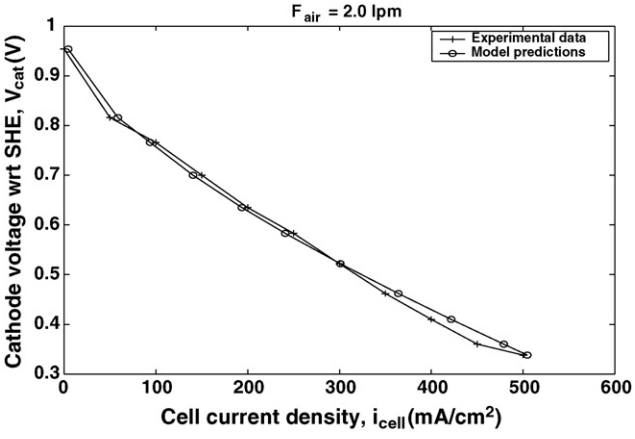

Fig. 13. Model predictions *vs.* experiment. F_{air} = 2.0 lpm.

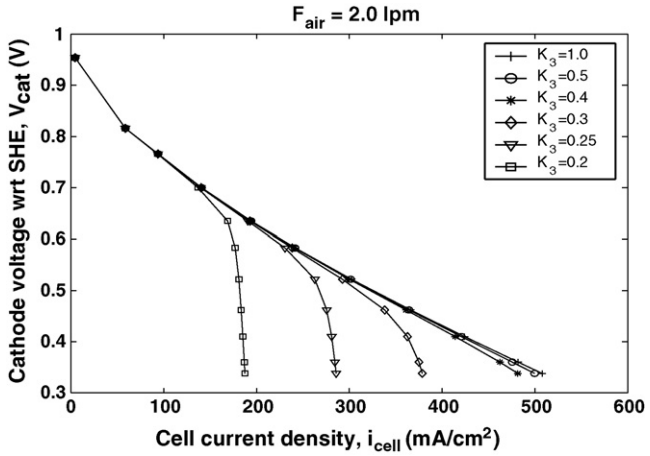

Fig. 14. Polarization curves for different values of K_3. $F_{air} = 2.0$ lpm.

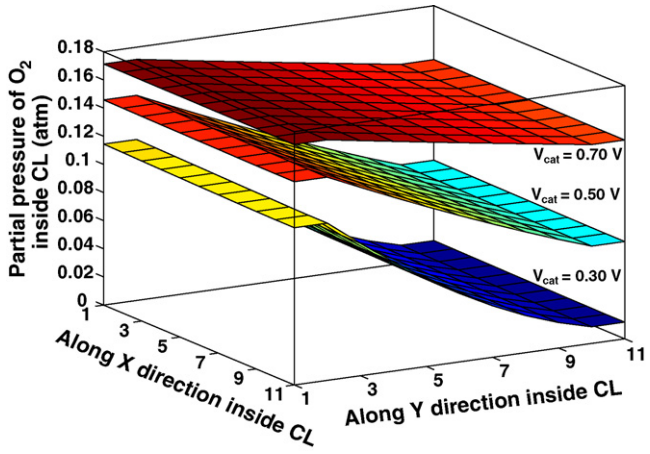

Fig. 15. Spatial variation of partial pressure of oxygen inside catalyst layer. $F_{air} = 0.20$ lpm.

around the spherical agglomerate increases, pushing the cell to a mass transfer limited regime. A similar study is carried out at the low flow rate of 0.2 lpm also. The nature of the plots do not change, but the cell reaches its limiting current density at a higher cell voltage than that of the simulations at 2.0 lpm for any given value of K_3. The simulation results clearly show that the interfacial liquid coverage plays a very important role in determining the limiting current density of a cell in a given operating condition.

5.2. Utility of the steady state model

The steady state cathode model can be used to study the effect of various inputs and design parameters (Table 3) on *i–v* characteristic curves. Inputs such as, flow rate of air, inlet pressure, inlet air humidity, inlet air temperature, and operating cell temperature can be considered. The effect of inlet air flow rate on *i–v* characteristic curve was already seen in Figs. 10, 12, and 13 during model validation. In addition, effect of design parameters such as, dimensions of the cell, catalyst loading (m_{pt}), weight fraction of platinum on carbon (f_{pt}), and weight fraction of ionomer inside catalyst layer (f_{mem}) can also be studied. Moreover, the steady state model can be used to study the spatial distribution of partial pressure or concentration of species, liquid water saturation, and ionomer phase potential inside different regions of the cathode. The effect of the operating cathode voltage on spatial distributions inside the catalyst layer is shown in Figs. 15–17 . Fig. 15 shows the spatial distribution of partial pressure of oxygen inside the catalyst layer for three different cathode voltages: $V_{cat} = 0.70, 0.50, 0.30$ V when inlet air flow rate is maintained at 0.2 lpm. For X direction inside catalyst layer, number "1" corresponds to microporous layer and the catalyst layer interface ($X = B$ in Fig. 2), and number "11" corresponds to the catalyst layer and the membrane interface ($X = C$ in Fig. 2). For Y direction inside the catalyst layer, number "1" corresponds to the inlet side ($Y = 0$ in Fig. 2) and number "11" corresponds to the outlet side ($Y = L$ in Fig. 2).

Fig. 16 shows the liquid water saturation inside the catalyst layer for the same three cathode voltages. We can see that when

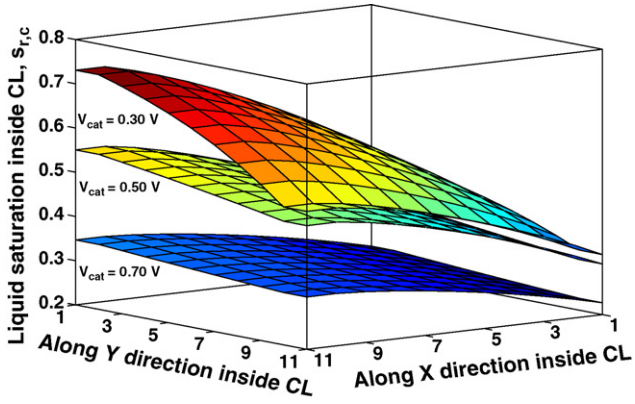

Fig. 16. Spatial variation of liquid water saturation inside catalyst layer. $F_{air} = 0.20$ lpm.

the cathode voltage is low (0.3 V), implying high potential driving force for the chemical reaction, there are regions inside the catalyst layer where 70% of the voids are filled with liquid water. The region inside the catalyst layer (number "1" along Y direction and number "11" along X direction) corresponds to control volumes near the membrane and the inlet. Fig. 17 shows the spatial variation of ionomer phase potential inside the catalyst

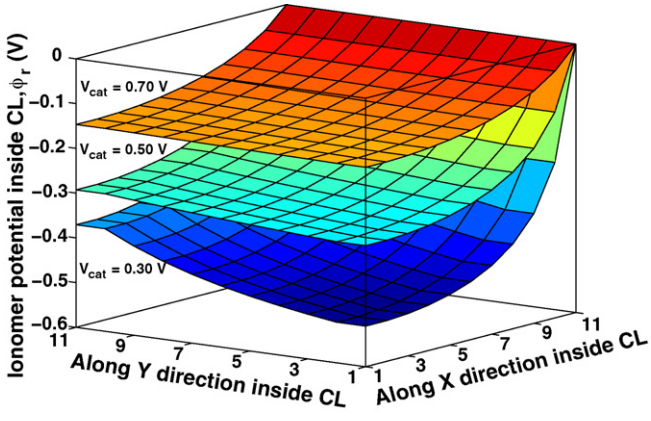

Fig. 17. Spatial variation of ionomer potential inside catalyst layer. $F_{air} = 0.20$ lpm.

layer. One can see that the gradients along the X direction become steeper when cathode voltage decreases from 0.70 to 0.30 V. It can be observed that all the three surface have a common edge at the top. This is due to the fact that the catalyst layer is interfaced with a standard hydrogen electrode for voltage measurements and this edge is taken as the reference.

Steady state models can be used to do optimization studies wherein some inputs or design parameters are allowed to vary within a range of values to maximize or minimize an objective and at the same time satisfying one or more criteria. In a related work [10], the steady state cathode model was used to study an optimization problem where the objective was to maximize the cell current density. In order to do this, catalyst loading (m_{pt}), weight fraction of platinum on carbon (f_{pt}), weight fraction of ionomer inside catalyst layer (f_{mem}), and catalyst layer thickness (t_{RL}) are treated as optimization variables. The details of the optimization formulation, numerical procedure and results are described in [10].

6. Conclusions

A two-dimensional steady state model for the cathode of a PEM fuel cell was presented in this work. Various modeling assumptions and catalyst layer characterizations were tested during model validation. It was shown that the model predictions using the spherical agglomerate characterization of the catalyst layer best fits the experimental data. An approach to correlate experimental conditions to model parameters was suggested. Using this correlation, it is possible to perform multi-parameter optimization studies for fuel cell systems. The results of such an optimization study is presented in [10]. Improvements to the model proposed in this paper can lead to the use of such models in design of fuel cell materials for better performance. It was also shown that the wettability of the different layers plays a very important role in getting the best performance out of a PEM fuel cell.

Acknowledgements

We would like to acknowledge American Chemical Society—Petroleum Research Fund (ACS-PRF) for providing financial support for this work. Grant # PRF 42842-AC9.

References

[1] J. Benziger, E. Chia, K.J. Moxley, C. Teuscher, I.G. Kevrekidis, The stirred tank reactor polymer electrolyte membrane fuel cell, AIChE J. 50 (8) (2004) 1889–1900.
[2] M. Eikerling, A.A. Kornyshev, A.R. Kucernak, Water in polymer electrolyte fuel cells: Friend or foe? Phys. Today (2006) 38–44.
[3] C.-Y. Wang, Fundamental models for fuel cell engineering, Chem. Rev. 104 (2004) 4727–4766.
[4] U. Pasaogullari, C.-Y. Wang, Liquid water transport in gas diffusion layer of polymer electrolyte fuel cells, J. Electrochem. Soc. 151 (3) (2004) A399–A406.
[5] G. Lin, W. He, T.V. Nguyen, Modeling liquid water effects in the gas diffusion and catalyst layers of the cathode of a PEM fuel cell, J. Electrochem. Soc. 151 (12) (2004) A1999–A2006.
[6] Y. Wang, C. Wang, Transient analysis of polymer electrolyte fuel cells, Electrochim. Acta 50 (2005) 1307–1315.
[7] E. Middleman, Improved PEM fuel cell electrodes by controlled self-assembly, Fuel Cells Bull. (2002) 9–12.
[8] S.J. Lee, S. Mukerjee, J. McBreen, Y.W. Rho, Y.T. Kho, T.H. Lee, Effects of Nafion impregnation on performances of PEMFC cathodes, Electrochim. Acta 43 (24) (1998) 3693–3701.
[9] F. Liu, B. Yi, D. Xing, J. Yu, Z. Hou, Y. Fu, Development of novel self-humidifying composite membranes for fuel cells, J. Power Sources 124 (2003) 81–89.
[10] R.M. Rao, R. Rengaswamy, S.R. Choudhury, Optimization of design parameters of the catalyst layer in the cathode of a proton exchange membrane fuel cell for performance, AIChE Annual Meeting, November 12–17, 2006, San Francisco,USA.
[11] D.M. Bernardi, M.W. Verbrugge, Mathematical model of a gas diffusion electrode bonded to a polymer electrolyte, AIChE J. 37 (8) (1991) 1151–1163.
[12] D.M. Bernardi, M.W. Verbrugge, A mathematical model of a solid-polymer-electrolyte fuel cell, J. Electrochem. Soc. 139 (9) (1992) 2477–2491.
[13] T. Berning, D.M. Lu, N. Djilali, Three-dimensional computational analysis of transport phenomena in a PEM fuel cell, J. Power Sources 106 (2002) 284–294.
[14] D. Bevers, M. Wohr, K. Yasuda, K. Oguru, Simulation of a polymer electrolyte fuel cell electrode, J. Appl. Electrochem. 27 (1997) 1254–1264.
[15] C.C. Boyer, R.G. Anthony, A.J. Appleby, Design equations for optimized PEM fuel cell electrodes, J. Appl. Electrochem. 30 (2000) 777–786.
[16] K. Broka, P. Ekdunge, Modelling the PEM fuel cell cathode, J. Appl. Electrochem. 27 (1997) 281–289.
[17] Y. Bultel, P. Ozil, R. Durand, Modelling the mode of operation of PEMFC electrodes at the particle level: influence of ohmic drop within the active layer on electrode performance, J. Appl. Electrochem. 28 (1998) 269–276.
[18] Y. Bultel, P. Ozil, R. Durand, Modelling of mass transfer within the PEM fuel cell active layer: limitations at the particle level, J. Appl. Electrochem. 29 (1999) 1025–1033.
[19] K. Dannenberg, P. Ekdunge, G. Lindbergh, Mathematical Model of the PEMFC, J. Appl. Electrochem. 30 (2000) 1377–1387.
[20] A. Dutta, S. Shimpalee, J.W. Van Zee, Three-dimensional numerical simualtion of straight channel PEM fuel cells, J. Appl. Electrochem. 30 (2000) 135–146.
[21] M. Eikerling, A.A. Korneyshev, Modelling the performance of the cathode catalyst layer of polymer electrolyte cells, J. Electroanal. Chem. 453 (1998) 89–106.
[22] V. Gurau, F. Barbir, H. Liu, An analytical solution of a half-cell model for PEM fuel cells, J. Electrochem. Soc. 147 (7) (2000) 2468–2477.
[23] V. Gurau, H. Liu, S. Kakac, Two-dimensional model for proton exchange membrane fuel cells, AIChE J. 44 (11) (1998) 2410–2422.
[24] W. He, J.S. Yi, T.V. Nguyen, Two-phase flow model of the cathode of PEM fuel cells using interdigitated flow fields, AIChE J. 46 (10) (2000) 2053–2064.
[25] G.J.M. Janssen, A phenomenological model of water transport in a proton exchange membrane fuel cell, J. Electrochem. Soc. 148 (12) (2001) A1313–A1323.
[26] J. Kim, S.-M. Lee, S. Srinivasan, C.E. Chamberlin, Modeling of proton exchange membrane fuel cell performance with an empirical equation, J. Electrochem. Soc. 142 (8) (1995) 2670–2674.
[27] A.A. Kulikovsky, J. Divisek, A.A. Kornyshev, Modeling the cathode compartment of polymer electrolyte fuel cells: dead and active reaction zones, J. Electrochem. Soc. 146 (11) (1999) 3981–3991.
[28] G. Maggio, V. Recupero, L. Pino, Modeling polymer electrolyte fuel cells: an innovative approach, J. Power Sources 101 (2001) 275–286.
[29] R.F. Mann, J.C. Amphlett, M.A.I. Hooper, H.M. Jensen, B.A. Peppley, P.R. Roberge, Development and application of a generalised steady-state electrochemical model for a PEM fuel cell, J. Power Sources 86 (2000) 173–180.
[30] H. Meng, C.Y. Wang, Model of two-phase flow and flooding dynamics in polymer electrolyte fuel cells, J. Electrochem. Soc. 152 (2005) A1733–A1741.

[31] G. Murgia, L. Pisani, M. Valentini, B. D'Aguanno, Electrochemistry and mass transport in polymer electrolyte membrane fuel cells. I. Model, J. Electrochem. Soc. 149 (1) (2002) A31–A38.
[32] D. Natarajan, T.V. Nguyen, A two-dimensional, two-phase, multicomponent, transient model for the cathode of a proton exchange membrane fuel cell using conventional gas distributors, J. Electrochem. Soc. 148 (12) (2001) A1324–A1335.
[33] U. Pasaogullari, C.-Y. Wang, Two-phase modeling and flooding prediction of polymer electrolyte fuel cells, J. Electrochem. Soc. 152 (2005) A380–A390.
[34] Y.W. Rho, S. Srinivasan, Y.T. Kho, Mass Transport phenomena in proton exchange membrane fuel cells using O_2/He, O_2/Ar, and O_2/N_2 Mixtures, J. Electrochem. Soc. 141 (8) (1994) 2089–2096.
[35] T.E. Springer, M.S. Wilson, S. Gottesfeld, Modeling and experimental diagnostics in polymer electrolyte fuel cells, J. Electrochem. Soc. 140 (12) (1993) 3513–3526.
[36] T.E. Springer, T.A. Zawodzinski, S. Gottesfeld, Polymer electrolyte fuel cell model, J. Electrochem. Soc. 138 (8) (1991) 2334–2342.
[37] D. Thirumalai, R.E. White, Mathematical modeling of proton-exchange-membrane fuel-cell stacks, J. Electrochem. Soc. 144 (5) (1997).
[38] S. Um, C.-Y. Wang, K.S. Chen, Computational fluid dynamics modeling of proton exchange membrane fuel cells, J. Electrochem. Soc. 147 (12) (2000) 4485–4493.
[39] Y. Wang, C.-Y. Wang, A non-isothermal, two-phase model of polymer electrolyte fuel cells, J. Electrochem. Soc. 153 (2006) A1193–A1200.
[40] Z.H. Wang, C.Y. Wang, K.S. Chen, Two-phase flow and transport in the air cathode of proton exchange membrane fuel cells, J. Power Sources 94 (2001) 40–50.
[41] J.S. Yi, T.V. Nguyen, An along-the-channel model for proton exchange membrane fuel cells, J. Electrochem. Soc. 145 (4) (1998) 1149–1159.
[42] J.S. Yi, T.V. Nguyen, Multicomponent transport in porous electrodes of proton exchange membrane fuel cells using thr interdigitated gas distributors, J. Electrochem. Soc. 146 (1) (1999) 38–45.
[43] L. You, H. Liu, A two-phase flow and transport model for the cathode of PEM fuel cells, Int. J. Heat Mass Trans. 45 (2002) 2277–2287.
[44] U. Pasaogullari, C.-Y. Wang, Two-phase transport and the role of microporous layer in polymer electrolyte fuel cells, Electrochim. Acta. 49 (2004) 4359–4369.
[45] J. Giner, C. Hunter, The mechanism of operation of the Teflon-bonded gas diffusion electrode: a mathematical model, J. Electrochem. Soc. 116 (8) (1969) 1124–1130.
[46] M.B. Cutlip, S.C. Yang, P. Stonehart, Simulation and optimization of porous gas-diffusion electrodes used in hydrogen/oxygen phosphoric acid fuel cells. II. Development of a detailed anode model, Electrochim. Acta 36 (3/4) (1991) 547–553.
[47] S.C. Yang, M.B. Cutlip, P. Stonehart, Simulation and optimization of porous gas-diffusion electrodes used in hydrogen/oxygen phosphoric acid fuel cells. I. Application of cathode model simulation and optimization of PAFC cathode development, Electrochim. Acta 35 (5) (1990) 869–878.
[48] H. Celiker, M.A. Al-saleh, S. Gultekin, S. Al-zakri, A mathematical model for the performance of raney metal gas diffusion electrodes, J. Electrochem. Soc. 138 (6) (1991) 1671–1681.
[49] M.A. Al-Saleh, S. Gultekin, S.U. Rahman, A. Al-Zakri, Modified flooded spherical agglomerate model for gas-diffusion electrodes in alkaline fuel cells, J. Power Sources 55 (1995) 33–39.
[50] M.L. Perry, J. Newman, E.J. Cairns, Mass transport in gas-diffusion electrodes: a diagnostic tool for fuel-cell cathodes, J. Electrochem. Soc. 145 (1) (1998) 5.
[51] S.R. Choudhury, M.B. Deshmukh, R. Rengaswamy, A two-dimensional steady-state model for phosphoric acid fuel cells (PAFC), J. Power Sources 112 (2002) 137–152.
[52] G. Maggio, Modelling of phosphoric acid fuel cell cathode behaviour, J. Appl. Electrochem. 29 (1999) 171–176.
[53] G. Lin, W. He, T.V. Nguyen, Modeling liquid water effects in the gas diffusion and catalyst layers of the cathode of a PEM fuel cell, J. Electrochem. Soc. 151 (12) (2004) A1999–A2006.
[54] N.P. Siegel, M.W. Ellis, D.J. Nelson, M.R. von Spakovsky, Single domain PEMFC model based on agglomerate catalyst geometry, J. Power Sources 115 (2003) 81–89.
[55] D. Song, Q. Wang, Z. Liu, T. Navessin, S. Holdcroft, Numerical study of PEM fuel cell cathode with non-uniform catalyst layer, Electrochim. Acta 50 (2004) 731–737.
[56] Q. Wang, M. Eikerling, D. Song, Z. Liu, Structure and performance of different types of agglomerates in cathode catalyst layers of PEM fuel cells, J. Electroanal. Chem. 573 (2004) 61–69.
[57] Q. Wang, D. Song, T. Navessin, S. Holdcroft, Z. Liu, A mathtematical model and optimization of the cathode catalyst layer structure in PEM fuel cells, Electrochim. Acta 50 (2004) 725–730.
[58] F. Gloaguen, P. Convert, S. Gamburzev, O.A. Velev, S. Srinivasan, An evaluation of the macro-homogeneous and agglomerate model for oxygen reduction in PEMFCs, Electrochim. Acta 43 (24) (1998) 3767–3772.
[59] F. Gloaguen, R. Durand, Simulations of PEFC cathodes: an effectiveness factor approach, J. Appl. Electrochem. 27 (1997) 1029–1035.
[60] H. Meng, C.-Y. Wang, Electron transport in polymer electrolyte fuel cells, J. Electrochem. Soc. 151 (2004) A358–A367.
[61] R.K. Shah, A.L. London, Advances in Heat Transfer, Supplement 1. Laminar Flow Forced Convection in Ducts, Academic Press, New York, 1978.
[62] T. Berning, N. Djilali, A 3D multiphase, multicomponent model of the cathode and anode of a PEM fuel cell, J. Electrochem. Soc. 150 (12) (2003) A1589–A1598.
[63] A.A. Kulikovsky, Quasi-3D modeling of water transport in polymer electrolyte fuel cells, J. Electrochem. Soc. 150 (11) (2003) A1432–A1439.
[64] J.M. Stockie, K. Promislow, B.R. Wetton, A finite volume method for multicomponent gas transport in a porous fuel cell electrode, Int. J. Numer. Meth. Fluids 41 (6) (2003) 577–599.
[65] C.N. Satterfield, Mass Transfer in Hetereogeneous Catalysis, MIT Press, Cambridge, 1970.
[66] R.B. Bird, W.E. Stewart, E.N. Lightfoot, Transport Phenomena, John Wiley & Sons Inc, New York, 1960.
[67] R. Rao, R. Madhusudana, Rengaswamy, Dynamic characteristics of spherical agglomerate for study of cathode catalyst layers in proton exchange membrane fuel cells (PEMFC), J. Power Sources 158 (2006) 110–123.
[68] W. Sun, B.A. Peppley, K. Karan, An improved two-dimensional cathode model to study the influence of catalyst layer structural parameters, Electrochim. Acta 50 (2005) 3359–3374.
[69] D. Natarajan, T.V. Nguyen, Three-dimensional effects of liquid water flooding in the cathode of a PEM fuel cell, J. Power Sources 115 (2003) 66–80.
[70] G. Lin, T.V. Nguyen, A two-dimensional two-phase model of a PEM fuel cell, J. Electrochem. Soc. 153 (2) (2006) A372–A382.
[71] F.Y. Zhang, X.G. Yang, C.Y. Wang, Liquid water removal from a polymer electrolyte fuel cell, J. Electrochem. Soc. 153 (2) (2006) A225–A232.
[72] J.C. Amphlett, R.M. Baumert, R.F. Mann, B.A. Peppley, P.R. Roberge, T.J. Harris, Performance modeling of the Ballard Mark IV solid polymer electrolyte fuel cell. 1. Mechanistic model development, J. Electrochem. Soc. 142 (1) (1995) 1–8.
[73] Z. Ogumi, Z. Takehara, S. Yoshizawa, Gas permeation in SPE method. I. Oxygen permeation through Nafion and NEOSEPTA, J. Electrochem. Soc. 131 (4) (1984) 769–773.
[74] A.C. West, T.E. Fuller, Influence of rib spacing in proton-exchange membrane electrode assemblies, J. Appl. Electrochem. 26 (1996) 557–565.
[75] T.E. Springer, T.A. Zawodzinski, M.S. Wilson, S. Gottesfeld, Characterization of polymer electrolyte fuel cells using ac impedance spectroscopy, J. Electrochem. Soc. 143 (2) (1996) 587–599.
[76] H. Ju, C.-Y. Wang, Experimental validation of a PEM fuel cell model by current distribution data, J. Electrochem. Soc. 151 (2004) 1954–1960.
[77] A. Parthasarathy, S. Srinivasan, A.J. Appleby, Temperature dependence of the electrode kinetics of oxygen reduction at the platinum/Nafion interface—a microelectrode investigation, J. Electrochem. Soc. 139 (9) (1992) 2530–2537.